Accepted refereed manuscript of:

Patton H, Hubbard A, Bradwell T & Schomacker A (2017) The configuration, sensitivity and rapid retreat of the Late Weichselian Icelandic ice sheet, *Earth-Science Reviews*, 166, pp. 223-245.

DOI: 10.1016/j.earscirev.2017.02.001

Manuscript Details

Manuscript number	EARTH_2016[redacted]
Title	The configuration, sensitivity and rapid retreat of the Late Weichselian Icelandic ice sheet
Article type	Review Article

Abstract

The fragmentary glacial-geological record across the Icelandic continental shelf has hampered reconstruction of the volume, extent and chronology of the Late Weichselian ice sheet particularly in key offshore zones. Marine geophysical data over the last two decades reveals that the ice sheet likely attained a continental shelf-break position in all sectors during the Last Glacial Maximum, though its precise timing and configuration remains largely unknown. Within this context, we review the available empirical evidence and use a well-constrained three-dimensional thermomechanical model to investigate the drivers of an extensive Late Weichselian Icelandic ice-sheet, its sensitivity to environmental forcing and phases of deglaciation. Our reconstruction attains the continental shelf break across all sectors with a total ice volume of 5.96 x 105 km3 with high precipitation rates being critical to forcing extensive ice sheet flow offshore. Due to its location astride an active mantle plume, a relatively fast and dynamic ice sheet with a low aspect ratio is maintained. Our results reveal that once initial ice-sheet retreat was triggered through climate warming at 21.8 ka BP, marine deglaciation was rapid and accomplished in all sectors within c. 5 ka at a mean rate of 71 Gt of mass loss per year. This rate of ice wastage is comparable to contemporary rates observed for the West Antarctic ice sheet. The ice sheet subsequently stabilised on shallow pinning points across the near shelf for two millennia, but abrupt atmospheric warming during the Bølling Interstadial forced a second, dramatic collapse of the ice sheet onshore with a net wastage of 221 Gt a-1 over 750 years, analogous to contemporary Greenland rates of mass loss. Geothermal conditions impart a significant control on the ice sheet's transient response, particularly during phases of rapid retreat. Insights from this study suggests that large sectors of contemporary ice sheets overlying geothermally active regions, such as Siple Coast, Antarctica, and NE Greenland, have the potential to experience rapid phases of mass loss and deglaciation once initial retreat is initiated.

Keywords	Iceland, Late Weichselian, ice sheet modelling, geothermal, collapse, palaeo reconstruction

Corresponding Author	Henry Patton
Order of Authors	Henry Patton, Alun Hubbard, Tom Bradwell, Anders Schomacker
Suggested reviewers	[redacted]
Opposed reviewers	[redacted]

1. Introduction

Reconstruction of the Late Weichselian extent and deglaciation history of the Icelandic Ice Sheet (IIS) has largely depended upon a relatively limited and sparsely distributed empirical record, especially in the marine sector (e.g., Norðdahl, 1991; Andrews et al., 2000; Norðdahl et al., 2008; Ingólfsson et al., 2010). Recent geomorphological mapping from shelf-wide acoustic bathymetric surveys has revealed an unprecedented view of the former glacial footprint in all sectors of the Icelandic continental shelf (Spagnolo and Clark, 2009), supporting previous insights from the landform and sediment record for the possibility of an extensive marine-terminating ice sheet at the Last Glacial Maximum (LGM) (Figure 1A) (Ólafsdóttir, 1975; Egloff and Johnson, 1979; Boulton et al., 1988; Syvitski et al., 1999). Previous ice-sheet modelling by Hubbard et al. (2006) revealed that substantial parts of the IIS were potentially marine-based during the LGM. However, equivocal and piecemeal chronological control across the continental shelf has not allowed a full understanding of the form and extent of the LGM ice sheet prior to its retreat into near-shore areas around 16 ka BP (e.g., Andrews et al., 2000; Jennings et al., 2000; Geirsdóttir et al., 2002; Norðdahl and Pétursson, 2005). From c. 16 ka onwards, radiocarbon dated raised beaches and marine sediments around the present Icelandic coastline, as well as an exceptionally high marine limit of c. 150 m a.s.l. at Stóri-Sandhóll in West Iceland (Ingólfsson and Norðdahl, 2001), indicate that deglaciation onto land occurred extremely rapidly, coinciding with a period of rapid eustatic sea-level rise during the meltwater pulse 1A event c. 15.0 ka BP (Ingólfsson and Norðdahl, 2001; Norðdahl and Ingólfsson, 2015).

As well as being a largely marine-based ice sheet, the Icelandic domain is of particular interest because of its unique position straddling the tectonically active Mid-Atlantic lithosphere plate boundary (**Figure 1**B). This ~8000 km long spreading centre not only delivers large fluxes of geothermal heat, but is also prone to frequent, large-scale volcanic eruptions (cf. Thordarson and Larsen, 2007). Geothermal heat supply to the subglacial environment can have a primary influence on ice sheet thermodynamics, through temperature-dependent softening of ice-fabric yielding

enhanced basal strain-rates, and/or through elevated levels of melting leading to widespread basal lubrication and motion. During episodes of vigorous subglacial volcanic activity, for example the regular eruptions at Grímsvötn, Bárðarbunga or Kverkfjöll (Óladóttir et al., 2011), the introduction of enhanced basal temperatures exerts a first-order control on ice sheet form, dynamics and stability. During such volcanic episodes, localised rates of subglacial melting exceeds mass-balance terms by an order of magnitude or more, triggering large-scale jökulhlaups (Gudmundsson et al., 1997; Geirsdóttir et al., 1999) promoting fast flow (e.g., Blankenship et al., 1993; Vogel and Tulaczyk, 2006).

The distribution of geothermal heat flux across Iceland peaks at over 300 mW m^{-2} within the neovolcanic zone, straddling the central rift from SW to NE Iceland (**Figure 1**B). This zone has experienced large variations in magma eruption rates during the last glacial cycle (Jakobsson et al., 1978; Vilmundardóttir and Larsen, 1986; Sigvaldason et al., 1992; Slater et al., 1998), with extrusive episodes 50 times more frequent during deglaciation compared to recent times (Jull and McKenzie, 1996; Maclennan et al., 2002). Previous modelling experiments and geophysical data from Iceland indicate that dramatic increases in eruption rates were associated with the onset of deglaciation and glacio-isostatic unloading (Jull and McKenzie, 1996; Slater et al., 1998; Maclennan et al., 2002; Geyer and Bindeman, 2011). However, discriminating the impact of spatial variations in the geothermal flux on the evolution and dynamics of the Icelandic ice-sheet are yet to be fully investigated from a numerical modelling perspective (Bourgeois et al., 2000). This research focus has wide significance given the large sectors of today's Polar ice sheets and smaller ice masses that are located over volcanically active zones characterised by high geothermal fluxes, for example, the Northeast Greenland ice stream (Fahnestock et al., 2001; Rogozhina et al., 2016), the East-West Antarctica boundary (Maule et al., 2005) and the Siple Coast ice streams (Fisher et al., 2015).

Here we present and examine a new model for the last glaciation of the Icelandic continental shelf within the context of recent chronological and geological insights – particularly in the light of improved shelf-wide geomorphological mapping of the offshore landform record – whilst also reconciling much of the previously published evidence. First, we review the existing empirical evidence that reliably constrains the advance and demise of the last ice sheet, including during the Younger Dryas stadial – a brief cold reversal that interrupted climate amelioration during deglaciation. We then present model output from an optimal experiment, that extends the coupled climate/ice-sheet-flow modelling of Hubbard et al. (2006), putting forward a robust and glaciologically plausible reconstruction of an extensive, marine-based Late Weichselian IIS that reached the continental shelf-edge in all sectors. From this reconstruction we highlight a number of key findings relating to the IIS, including: zonal flow configurations; potential drivers of collapse; as well as its sensitivity and response to a range of internal and external drivers, including the effects of spatially variable geothermal heat flow.

2. The empirical record of glaciation

In this section we review the key morphological and chronological evidence for ice-sheet glaciation across the Icelandic continental shelf during the LGM, providing a context in which to place our new modelling results. We assume the LGM of Iceland to have been coeval with the global ice-sheet maximum, which occurred between 26.5-19 ka BP (Peltier and Fairbanks, 2006; Clark et al., 2009). This period is widely referred to as the Late Weichselian glaciation (Europe) (Ingólfsson, 1991; Norðdahl, 1991), equivalent to the Late Wisconsinan of North America, or Late Devensian of the United Kingdom. Offshore, marine geologists commonly use Marine Isotope Stages (MIS) to refer to alternating warm and cold periods – in this case the main Late Weichselian Stadial (and LGM) is associated with MIS2 (29-14 ka BP), proceeding the previous interstadial in MIS3 (60-29 ka BP).

Reported ^{14}C ages are recalibrated in this paper to calendar years before present (cal. ka BP) using the program Calib 7.1 (Stuiver and Reimer, 1993) and the IntCal13/MARINE13 calibration curves (Reimer et al., 2013). The marine calibration incorporates a time-dependent global ocean reservoir correction of about 400 years, with a ΔR value of 24±23 used to accommodate local effects (Håkansson, 1983).

2.1. Onset of shelf glaciation (MIS 3/2 transition)

Few data constrain the timing or extent of glaciation prior to the LGM, though it is generally assumed the IIS was not on the shelf during the latter part of MIS 3 (Norðdahl and Pétursson, 2005; Andrews, 2008). A till of Mid Weichselian age has been reported from Suðurnes on the Reykjanes peninsula based on two samples dated to c. 31.6 cal. ka BP found within overlying marine sediments (Eiríksson et al., 1997). Based on these dates and sediments, it can be inferred that the southwest coastline was probably ice free during the late Mid Weichselian, tentatively correlated with similar restricted ice-cover in western Norway during the Ålesund interstadial (Figure 1) (Mangerud et al., 1981, 2010). West of Keflavík, till containing fossiliferous sediment clasts overlying striated (215°) bedrock has yielded an age of c. 28.1 cal. ka BP, providing a maximum age for the advance of Late Weichselian ice in this region. However, a weighted mean age from six marine shell samples within stratified sands resting on glacially striated (009°) bedrock north of Rauðamelur suggests that shallow marine conditions may have persisted here until c. 25.8 cal. ka BP (cf. Norðdahl and Pétursson, 2005).

2.2. Last Glacial Maximum (28.1-22.8 cal. ka BP)

2.2.1. The timing of maximum extension

For a significant time, constraining the maximum extent of former ice beyond the present-day coastline was limited to observations from islands or low-resolution snapshots of offshore seismic data. Early reports of till, drumlins, roches moutonnées, striae and meltwater channels on the island of Grímsey 40 km off northern Iceland, confirm that ice overrode, and was thick enough to cover the

highest parts of the island (> 100 m), at least once (Keith and Jones, 1935; Hoppe, 1968). Although not constrained by any numerical ages, the well preserved meltwater channels and apparent absence of either solifluction cover or of older soils over the thin till deposits, together, were used to suggest a LGM age (Hoppe, 1968).

The first description of a submarine glacial landform on the Icelandic continental shelf was reported by Ólafsdóttir (1975), with the discovery of a prominent moraine-like ridge at the western continental shelf break. This feature extends for more than 100 km, lies at water depths of between 200-350 m, and is typically 20 m in relief although in places can reach more than 100 m high (Syvitski et al., 1999) (**Figure 1**A). A core collected seaward of this Látra Bank end-moraine has provided a maximum age of this deposit of c. 40.2 ka BP, although dating material was possibly collected from a pre-LGM erosion surface here (Syvitski et al., 1999). Basal dates from further cores on the adjacent upper shelf have provided ages of c. 21.4 and 21.6 cal. ka BP, and although do not confirm or refute the presence of LGM ice at the moraine, imply only modest sediment accumulation rates were achieved in this sector (10.2 cm kyr^{-1}) (Andrews et al., 2000). Compared with an upper shelf slope core taken from the opposite side of the Denmark Strait, below the mouth of Kangerlussuaq Trough, the accumulation rates in the Icelandic sector are three times lower (30.6 cm kyr^{-1}) (Andrews et al., 1998). Andrews et al. (2000) therefore suggested that the western Icelandic ice sheet margin was either not a major contributor of sediment to the upper slope, or that the area was by-passed by various downslope transport processes during the LGM (e.g., Syvitski et al., 1999).

Further geophysical surveying offshore has revealed major till deposits up to 100 m thick at the continental shelf edge in the south-eastern sector, as well as an associated retreat moraine complex – the Tvísker moraine – 20 km from the present coastline (Boulton et al., 1988). Off southwestern Iceland, Egloff and Johnson (1979) also found an acoustically transparent, 100-350 m thick upper layer present adjacent to the shelf edge. With no chronological control, this sediment package,

123 resting on a probable erosional surface, was interpreted to represent morainic deposits of Late
124 Pleistocene age.

125 More recent, systematic coring efforts north and northwest of Iceland have attempted to pinpoint
126 the LGM ice sheet extent on the continental shelf, though results proved largely equivocal. Three
127 cores recovered from within Reykjafjarðaráll, a large trough extending from north Iceland towards
128 the shelf break, revealed a broad cover of matrix-supported diamicton overlain by fine-grained
129 postglacial muds (Andrews and Helgadóttir, 2003). All foraminifera samples within the lower
130 diamicton provided consistently old dates (27-44 cal. ka BP), while radiocarbon dates immediately
131 above the diamicton yielded ages of c. 13 cal. ka BP. The preferred interpretation by these authors
132 was that the stratigraphy and chronology could be best explained by Late Weichselian ice
133 overrunning the sites, reworking glacio-marine sediments deposited >25 cal. ka BP, and persisting in
134 the trough until c. 13 cal. ka BP (Andrews and Helgadóttir, 2003; Principato et al., 2005). Based on
135 this conclusion, the core locations thus represent a minimum spatial constraint of the maximum Late
136 Weichselian ice-sheet margin.

137 An alternative interpretation for the "old" (> 25 cal. ka BP) lower diamicton is that it represents *in*
138 *situ* glacio-marine sediments that did not directly interact with an ice sheet, thus delimiting the
139 maximum spatial extent of the LGM ice sheet. Despite an absence of geomorphological evidence,
140 such as end-moraines or grounding-zone features within Reykjafjarðaráll to support a "restricted"
141 LGM ice sheet in this sector (Andrews and Helgadóttir, 2003; Spagnolo and Clark, 2009), this view
142 has generally persisted within the literature and has formed maximal constraints for a number of
143 conceptual and numerical reconstructions (Andrews et al., 2000; Norðdahl and Pétursson, 2005;
144 Hubbard et al., 2006; Norðdahl and Ingólfsson, 2015).

145 Djúpáll, a narrow cross-shelf extending northwest from Vestfirðir is traversed by a number of
146 prominent moraines, mapped from seismic profiles (Andrews et al., 2002); and seen on singlebeam
147 (Olex) bathymetric data (Spagnolo and Clark, 2009). Two anomalously "old" (> 35 cal. ka BP) dates

148 from foraminifera found within a massive diamict underlying laminated marine deposits have been
149 similarly used to infer a restricted LGM ice sheet on the NW shelf (Andrews et al., 2002b; Geirsdóttir
150 et al., 2002). However, more recent data has cast doubt on this interpretation, based on the
151 probability that the dated foraminifera from the underlying diamict here are also reworked
152 (Quillmann et al., 2009). Taking this into account, one corrected radiocarbon date of 22.8 cal. ka BP
153 from massive to faintly laminated glacimarine sediments (in core B997-338PC) provides a useful
154 minimum constraint for the retreat of the LGM ice sheet in this sector (Andrews et al., 2002b;
155 Geirsdóttir et al., 2002). Further basal core dates in the same part of the trough imply an average
156 sediment accumulation rate of around 30 cm kyr^{-1} during deglaciation (Andrews et al., 2000).

157 From an overview of the existing radiocarbon chronology offshore, it is clear that dating control on
158 the maximum extent of the LGM ice sheet is loose and spatially incoherent (Figure 1). Despite a
159 number of ages being affected by glacial reworking of the sediments, two dated cores from the
160 western sector of the ice sheet constrain a maximum and minimum age for the timing of ice advance
161 and retreat, indicating that Late Weichselian peak ice extent was probably attained sometime
162 between 25.8 and 22.8 cal. ka BP (Andrews et al., 2002b; Geirsdóttir et al., 2002).

163 ### 2.2.2. Shelf-edge glaciation?

164 A significant advance in our understanding of the offshore glacial footprint came with the release of
165 a bathymetric database compiled, processed and managed by Olex AS. The Olex bathymetric
166 database and resulting imagery is based upon single-beam echo-sounding, mostly derived from
167 fishing vessels, with a vertical resolution of ±1 m in water depths > 100 m, and 0.1 m at depths < 100
168 m. The horizontal positional error is limited by the precision of non-corrected, on-board Global
169 Positioning Systems, but is generally ~10 m and is further reduced by the cross-correlation of
170 multiple, coincident soundings. Mapping from this dataset allowed an unprecedented synoptic view
171 of glacial landforms on c. 80% of the continental shelf around Iceland. From this dataset, Spagnolo &
172 Clark (2009) mapped several hundred newly identified landforms, including submarine end moraines

and streamlined bedforms, which comprise the broad-scale glacial footprint of IIS extent and subsequent retreat.

The recent release of the EMODnet Digital Terrain Model – a composite bathymetric dataset, with data gaps filled using the GEBCO 2014 30" dataset to a horizontal resolution of 7.5 arc seconds (http://www.emodnet-hydrography.eu/) – has since provided complete bathymetric coverage of the Icelandic continental shelf at a resolution suitable for mapping large glacial landforms. Here, we consolidate and extend previous mapping offshore (Ólafsdóttir, 1975; Boulton et al., 1988; Spagnolo and Clark, 2009) with prominent features observed from Landsat imagery onshore as well as new landforms observed from previous data gaps offshore (**Figure 2**). The geomorphological interpretations made here are guided by the context of previous work described above.

The largest and most prominent geomorphological features on the continental shelf are a radial system of overdeepened cross-shelf troughs that extend from major onshore valley systems and widen towards the continental shelf edge. Compared to other cross-shelf troughs in high-latitude settings, such as around Greenland, Norway and northeast Canada, they are relatively shallow, and are draped with a thin layer of deglacial sediments, indicative of moderate rates of glacial erosion (Syvitski et al., 1987; Andrews et al., 2000). Most Icelandic cross-shelf troughs terminate with a reverse slope in long-profile and a bulging, arcuate terminus in planform (**Figure 2**C). Their association with distinct sets of large submarine streamlined ridges, running parallel to trough axes, as well as similar streamlined mega-lineations and striae onshore (Norðdahl, 1991; Bourgeois et al., 2000; Principato et al., 2016), strongly suggest that these areas were regions of streaming ice flow, indicative of widespread temperate subglacial conditions. Often associated with these offshore mega-lineations, are parallel channels up to 75 m in depth, 3 km wide and 20 km long, found incising to depths of 360 m below present-day sea level. Based on their morphological affinity with glacial channels elsewhere, and their location within zones of former temperate-based ice, these features

197 are likely to have formed by meltwater erosion during repeated episodes of grounded ice-sheet
198 advance (e.g. Ó Cofaigh, 1996).
199
200 Broad and well-defined features interpreted as moraines are located near the Icelandic shelf edge in
201 most sectors (**Figure 2**), of which two features have been previously identified though not
202 radiocarbon dated directly (Ólafsdóttir, 1975; Boulton et al., 1988; Syvitski et al., 1999) (Figure 1).
203 Moraine ridge lengths range from 6 to ~80 km, and their arcuate form is typical of end moraines
204 formed at grounded terrestrial ice-sheet margins. However, it cannot be completely discounted that
205 some of the ridges could represent subaqueous morainal banks – the product of grounded, quasi-
206 stable, water-terminating glaciers. A large ridge running parallel to the trough axis north of
207 Tröllaskagi is interpreted to be a medial-type moraine, formed at the junction of converging ice flow
208 units and downglacier of a topographic high.
209
210 Included in this landform group are a set of prominent ridges to the north of Vestfirðir (**Figure 2**B),
211 not previously described before in the literature due to bathymetry data gaps. Although the timing
212 of glaciation is still poorly constrained, their position adjacent to the shelf edge (consistent with
213 other sectors of the continental shelf), the northerly continuation of mapped MSGLs in nearby
214 troughs, the presence of perennial-sea ice cover stabilising calving margins around Iceland during
215 stadial conditions (Hoff et al., 2016), and the presence of subglacially reworked glacial diamicton in
216 present-day water depths of at least 347 m (Andrews et al., 2000) all indicate that grounded ice
217 during the Late Weichselian was probably more extensive in this sector than has been previously
218 speculated (Andrews et al., 2000; Norðdahl and Pétursson, 2005; Hubbard et al., 2006; Norðdahl and
219 Ingólfsson, 2015).Additional sets of arcuate moraines are present closer to the present day Vestfirðir
220 shoreline, demarcating potential still-stands or re-advances of the ice-sheet margin during
221 deglaciation (**Figure 2**) (Andrews et al., 2002b). Many of these moraines are associated with

extensive iceberg keel scouring mapped to depths of 180 m below present sea-level (Syvitski et al., 1999).

Despite a widespread coverage of glacial landforms across the continental shelf, limited marine coring combined with significant reworking of sediments during the last glacial cycle offshore (e.g Syvitski et al., 1999; Andrews et al., 2000; Andrews and Helgadóttir, 2003; Principato et al., 2005) means that robust chronological constraints on the extension of the LGM ice sheet are, unfortunately, lacking. Notwithstanding this poor chronological control, the geomorphological footprint of shelf-edge glaciation in all sectors, including newly identified moraine ridges north of Vestfirðir (**Figure 2**C), leaves extensive ice cover in all sectors as the most probable and compelling scenario for Late Weichselian glaciation over Iceland.

Further support for an extensive shelf-edge IIS configuration comes from the maximal extents of neighbouring mid-to-high-latitude ice sheets in the North Atlantic region at LGM. The most recent compilation of dates and reconstructions of the Eurasian Ice Sheet (Hughes et al., 2016) places the "most credible" ice sheet limits at, or close to, the continental shelf break at LGM (c. 27 ka) in the British/North Sea, Norwegian and Svalbard/Barents Sea sectors. Although dating control in these marine sectors is still not particularly firm, the compelling convergence of several lines of evidence (i.e. submarine geomorphology, seismic stratigraphy, seabed cores, ice-rafted debris records, and key dates) (cf. Ottesen et al., 2002; Clark et al., 2012; Patton et al., 2015) with updated numerical modelling (e.g., Hubbard et al., 2009; Patton et al., 2016) strongly suggest a shelf-edge scenario for the Eurasian ice-sheet complex at the LGM. Across the Denmark Strait, the southeastern sector (60-68°N) of the Greenland Ice Sheet also extended to the continental shelf edge at its Late Weichselian maximum (Roberts et al., 2008; Dowdeswell et al., 2010; Vasskog et al., 2015), with major ice streams supplying sediment to trough-mouth fans on the continental slope. Even the small and dynamic ice cap on the Faroe Islands is believed to have fed shelf-edge depocentres at maximum extent during the LGM (Nielsen et al., 2007).

2.2.3. Ice thickness

Onshore in Iceland, table mountains, erosional trimlines and glacial striae have all been used to reconstruct overall ice sheet thickness (Walker, 1965; Einarsson, 1968; Hjort et al., 1985; Norðdahl, 1991; Van Vliet-Lanoë et al., 2007). An extensive suite of cosmogenic ^{3}He exposure ages derived from table mountain summits within the neovolcanic zone provide an excellent constraint for ice-thickness changes during deglaciation (Licciardi et al., 2007). Moreover, if the exposure ages correctly date the timing of deglacial eruptions, the table mountain elevations also provide minimum altitudes for the LGM ice surface. These range from Herðubreið (1682 m a.s.l.) beneath the probable central ice divide, to Hafrafell (512 m a.s.l.) at the present-day northeast coastline (Licciardi et al., 2007).

The Tröllaskagi highlands have historically been the focus of numerous attempts to delimit ice-sheet thickness at the LGM. Based on geomorphological features such as lateral moraines, meltwater channels, upper limits of glacial erosion, and differences in weathering, a concept for maximum Weichselian glaciation in North Iceland was proposed that included significant ice-free areas interspersed by low gradient and interconnected ice streams (Norðdahl, 1991). Furthermore, the dendritic nature of the Tröllaskagi valley system was cited as evidence for glaciation by independent local ice domes rather than invasion from an inland ice sheet (Norðdahl, 1991). The existence of purported unglaciated coastal mountain areas, such as in the Tröllaskagi highlands, has also been cited as evidence in support of possible refugia sites for hardy plant species through the Weichselian – helping to explain the relatively high Holocene species diversity (e.g., Rundgren and Ingólfsson, 1999).

It is worth noting that previous model experiments, where the extent of Late Weichselian ice is limited at Grímsey, can reproduce ice-free areas across the Tröllaskagi highlands. However, modelled ice thicknesses vary significantly, by up to +63%, with perturbations in input parameters,

boundary conditions and modelled extent (Hubbard et al., 2006). Studies from around Europe have shown that distinguishing between zones that were completely ice-free and those protected by cold based/non-erosive ice based on geomorphology alone is a complex task, with ice-sheet thicknesses often underestimated (Fabel et al., 2002; Ballantyne, 2010). Unfortunately, the predominantly basaltic bedrock of Iceland precludes the collection of common paired cosmogenic isotopes (e.g., ^{10}Be and ^{26}Al) for determining complex exposure histories from mountain summits.

Deglacial cosmogenic ^{36}Cl exposure ages from erratic boulders in Vestfirðir are spread across the interval from 26 to 15 ka BP, indicating that the LGM ice sheet could have reached its maximum prior to this time; subsumed summits to at least 650 m a.s.l., and probably extended a considerable distance beyond the present-day coastline around northwest Iceland (Brynjólfsson et al., 2015). Brynjólfsson et al. (2015) interpreted the presence of erratic boulders sitting on top of an undisturbed block field as evidence of cold-based LGM ice over the uplands of Vestfirðir. Their conceptual model indicates warm-based ice in the lowlands as witnessed by the fjords, glacially eroded valleys, and widespread evidence of subglacial erosion.

2.3. Deglaciation (<22.8 cal. ka BP)

Dated glacimarine sediments in cores from Djúpáll reveal deglaciation was underway on the outer shelfby 22.8 cal. ka BP and had retreated to the mid shelf before 18.5 cal. ka BP (Andrews et al., 2000, 2002b). Furthermore, a basal date from marine sediments in a core north of Grímsey indicates that Atlantic Waters were present on the northern shelf >16.5 cal. ka BP (Eiríksson et al., 2000).

Onshore, cosmogenic exposure ages from glacially eroded bedrock in northern Vestfirðir strongly suggest that thinning of the ice sheet was underway soon after the LGM. Two samples collected from bedrock on Ármúli (Ísafjarðardjúp - 370 m a.s.l.) have produced an average ^{36}Cl age of 22.3 ka (20.4 ka with atmospheric correction) (Principato et al., 2006), whilst exposure ages from high-elevation erratic boulders on Leirufjall suggest ice-sheet thinning over Vestfirðir started as early as c. 26 cal. ka BP (Brynjólfsson et al., 2015). The ages of Principato et al. (2006) and Brynjólfsson et al.

298 (2015) are, however, not directly comparable because of the different production rates and scaling
299 parameters used in these respective studies.

300 ### 2.3.1. Bølling - Allerød (15.4 – 13.0 cal. ka BP)

301 Seismic profiling and sediment core studies indicate that deglaciation of the Icelandic continental
302 shelf between c. 15-13 cal. ka BP occurred rapidly (Syvitski et al., 1999; Jennings et al., 2000;
303 Andrews and Helgadóttir, 2003; Andrews, 2005), coeval with the northward migration of the Polar
304 Front as well as rapidly rising eustatic sea-levels during the Bølling interstadial (Ingólfsson et al.,
305 1997; Eiríksson et al., 2000; Ingólfsson and Norðdahl, 2001; Lambeck et al., 2014). Over the course of
306 a few centuries between c. 14.7-14.3 cal. ka BP global sea-levels underwent a period of massive
307 change, rising on average at a rate greater than 40 mm per year (Deschamps et al., 2012). Referred
308 to as meltwater pulse 1A, this event was probably a significant driver for the destabilisation of
309 marine-terminating glaciers around Iceland (Norðdahl and Ingólfsson, 2015).

310 Geological evidence for rapid retreat at this time in part comes from the relatively thin drape of
311 deglacial marine sediments over the continental shelf (Principato et al., 2005; Andrews, 2007;
312 Geirsdóttir et al., 2007), but is also supported by a number of key chronological constraints. Dates
313 from the near base of glacimarine sediments in Jökuldjúp (15.1-14.9 cal. ka BP; Jennings et al., 2000;
314 Principato et al., 2005) and in northward flowing troughs of Húnaflóadjúp (16.1-15.6 cal. ka BP;
315 Andrews and Helgadóttir, 2003; Principato et al., 2005) indicate ice-free conditions offshore by this
316 time (**Figure 1**B). Similarly aged radiocarbon dates in western Iceland, usually associated with high
317 raised marine shorelines (105-150 m a.s.l.), provide strong evidence that coastal areas here were
318 deglaciated and still submerged between c. 15.0-14.7 cal. ka BP (Ashwell, 1975; Geirsdóttir and
319 Eiriksson, 1994; Ingólfsson and Norðdahl, 2001; Norðdahl and Pétursson, 2005; Norðdahl and
320 Ingólfsson, 2015), also indicating a potentially catastrophic collapse of the near-shelf sectors of
321 Jökuldjúp. A further onshore date of 14.9 cal. ka BP constrains a Bølling marine transgression c. 60 m
322 a.s.l. in northeast Iceland (Norðdahl and Pétursson, 2005), with additional Bølling-aged raised marine

shorelines reported on the Reykjanes peninsula (70 m a.s.l.), Breiðafjörður (90-110 m a.s.l.), Vestfirðir (75-95 m a.s.l.), and the Skagi peninsula (65 m a.s.l.) (cf. Norðdahl and Pétursson, 2005). Given the generally low viscosity of the Iceland lithosphere and asthenosphere, it has been additionally argued that the very high elevations of these raised shorelines could only have formed under extremely rapid deglaciation (Ingólfsson and Norðdahl, 2001).

More quantitative support for this observation has come recently from cosmogenic-nuclide exposure-age dating of table mountain summits within the Iceland neovolcanic zone . The premise that a pulse of enhanced volcanic production immediately followed deglaciation has existed for some time, although the timing and mechanistic link is not well constrained (Jakobsson et al., 1978; Vilmundardóttir and Larsen, 1986; Sigvaldason et al., 1992; Slater et al., 1998; Maclennan et al., 2002; Sinton et al., 2005). However, the mean ages of 42 individual cosmogenic-exposure ages from 13 different table mountains within the neovolcanic zone reveal two discrete intervals of active table mountain growth at c. 14.4-14.2 ka and 11.1-10.5 ka, suggesting that these periods were associated with episodes of rapid ice-sheet thinning or unloading that stimulated enhanced volcanic activity (Licciardi et al., 2007).

Towards the end of the Bølling-Allerød Interstadial and onset of the Younger Dryas Stadial, the IIS began to expand once more. This period is marked by rising relative sea levels and general cooling of the marine environment – witnessed by the appearance of High Arctic mollusc species in western Iceland (Norðdahl and Pétursson, 2005). Rapid isostatic uplift of the crust in response to the swift collapse of marine-based ice-sheet sectors (e.g., Sigmundsson, 1991; Ingólfsson et al., 1995) may also have contributed to a regional relative lowering of the equilibrium-line altitude of the ice sheet, thus enhancing snow accumulation, ice sheet growth and glacier advance.

2.3.2. Younger Dryas & Early Holocene (13.0-10.0 cal. ka BP)

Truncated raised shorelines in the mouths of fjords and valleys around Iceland demonstrate that the ice sheet expanded during the Younger Dryas across many coastal sites that had been ice-free since Bølling deglaciation (Norðdahl and Pétursson, 2005; cf. Ingólfsson et al., 2010). In northern Iceland the ice sheet extended offshore into various fjords during the Younger Dryas, although elsewhere it was generally less extensive than the present-day coastline (Norðdahl and Haflidason, 1992; Geirsdóttir et al., 2000; Principato et al., 2006; Brynjólfsson et al., 2015) (**Figure 1**). Truncated shorelines of probable Younger Dryas age suggest that the tip of the Langanes Peninsula remained ice free during this stadial, with the glacier margin some 5 km inland from the present coast (Norðdahl and Hjort, 1995). Marine shorelines of an assumed Younger Dryas age between 58 and 35 m a.s.l. in eastern Iceland also suggest ice was grounded in the heads of the eastern fjords, with many promontories and headlands remaining ice-free (Norðdahl and Einarsson, 2001).

A prominent example of interrupted retreat of the IIS during the Lateglacial period is the Búði moraine system in south-central Iceland – a composite feature of multiple, discontinuous ridges. Most of this complex shows deltaic characteristics with distinct foreset bedding and glaciofluvial sandur accumulation, indicating a transition between marine-coastal and terrestrial environments and demonstrating that the southern lowlands of Iceland were submerged at the time of deposition (Hjartarson and Ingólfsson, 1988; Geirsdóttir et al., 1997, 2000). The occurrence of 11.98 ka BP Vedde Ash in forefield lake sediments, an extensive tephra marker layer associated with the pyroclastic eruption of Katla (Grönvold et al., 1995), along with *in situ* radiocarbon dates (Table 1) support a Younger Dryas age for the Outer Búði moraine c. 12.1-11.9 ka BP (Geirsdóttir et al., 1997; Norðdahl and Pétursson, 2005; Geirsdóttir, 2011). In central Iceland, cosmogenic exposure ages from table mountains reveal inland ice thickness at this time was c. 550 m (Licciardi et al., 2007).

Offshore ice-rafted debris records from cores within Ísafjarðardjúp reveal that calving glaciers were present on Vestfirðir from the Younger Dryas through to the earliest Holocene – known as the

Preboreal (ca. 11 ka BP), with submerged moraines in fjords appearing to support stepwise retreat of this margin (Geirsdóttir et al., 2002). More recent exposure-age dating appears to show that glacier retreat was asynchronous between various northwest fjords between the Allerød and Holocene, with time lags of up to 2-5 ka (Principato et al., 2006; Brynjólfsson et al., 2015). The abrupt climatic termination of the Younger Dryas Stadial (Dansgaard et al., 1989) prompted widespread retreat of the residual IIS, inducing rapid glacio-isostatic rebound (Norðdahl and Einarsson, 2001) that triggered a short-lived volcanic eruptive phase (Licciardi et al., 2007) as well as falling relative sea-levels.

The last, short-lived, advance of the IIS occurred during climate deterioration within the earliest Holocene or Preboreal (c. 11.2 cal. ka BP) (Rundgren et al., 1997; Norðdahl and Einarsson, 2001). Like the Younger Dryas, reconstruction of the ice extent at this time comes largely from the distribution of raised shorelines and ice-marginal landforms, and tephrochronological correlations, associated with a 20-25 m RSL transgression (Ingólfsson et al., 1995, 2010; Norðdahl and Pétursson, 2005). The first island-wide palaeoglaciological reconstruction by Norðdahl and Pétursson (2005) of this time interval reveals an ice sheet only c. 20% smaller than the Younger Dryas ice sheet and with a similar configuration. For example, the Inner Búði moraine system was formed during a Preboreal advance from 11.5-10.1 ka BP, with dated marine molluscs found both in front of and behind the moraine complex (Hjartarson and Ingólfsson, 1988; Geirsdóttir et al., 1997; Norðdahl and Pétursson, 2005). The greatest differences though lie in the major outlet glaciers of northern Iceland, which had retreated some 30-50 km from the mapped Younger Dryas limits.

By 10.3 ka BP, the main ice sheet had all but disappeared across the Icelandic highlands. This is confirmed by the presence of the Saksunarvatn tephra (c. 10.2 ka, Grönvold et al., 1995; Andrews et al., 2002a) in a number of high-elevation sites, including glacial lake Hvítárvatn (Stötter et al., 1999; Caseldine et al., 2003; Geirsdóttir et al., 2009; Larsen et al., 2012).

3. The ice flow model

Here we use a 3D, time-integrated ice sheet model based on the conservation of mass and heat utilizing Glen's (1955) flow law implemented under a first-order approximation of the Stokes-equations adopted from Blatter (1995), Hubbard (1999, 2000), Marshall et al. (2005), and Pollard and DeConto (2007). It has previously been applied to Iceland (Hubbard, 2006; Hubbard et al., 2006), the British Isles (Golledge et al., 2008; Hubbard et al., 2009; Patton et al., 2013), Patagonia (Hubbard et al., 2005) and the Eurasian ice-sheet complex (Patton et al., 2016) to investigate the build-up, extent and deglaciation of the palaeo-ice sheets that occupied these regions. The approach to solving the membrane stress and associated strain fields equate to the L1L2 classification of higher-order models defined by Hindmarsh (2004) that includes longitudinal deviatoric stresses that act to stabilise ice flow over steep relief with high rates of basal lubrication and motion. The model is thermomechanically coupled and temperature-dependent internal flow (ice deformation) is complimented by basal motion calculated using Weertman's (1964) sliding relation when subglacial temperatures attain pressure melting point. The model performs well when compared with second-order and full-Stokes schemes in the ISMIP-HOM benchmark experiments (Pattyn et al., 2008) and has been applied and validated against surface and englacial velocity measurements at Haut Glacier d'Arolla (Hubbard et al., 1998) and Glacier de Tsanfleuron (Hubbard et al., 2003; Chandler et al., 2006) under variable ice rheology. Model derivation, assumptions, limitations and implementation are found in the references above and description here is limited to specific implementation for Iceland.

The model requires key input data and boundary conditions: (i) the present-day reference climate comprising monthly mean air temperature (MMAT) and precipitation, (ii) relaxed basal topography, and (iii) the geothermal heat flux. The model is integrated forward through time from an initial (ice-free) condition and is forced through a time-series of temperature, precipitation and eustatic sea-level perturbations. Key parameters, constants and values are presented in Table 2.

421

422 ### 3.1. Climate and mass balance

423 Surface mass balance, which accounts for ice gains and losses from the ice-sheet surface, is
424 determined by a positive degree-day (PDD) scheme, applied according to Laumann and Reeh (1993),
425 and derives total melt from integrated monthly positive temperatures. Monthly temperature is
426 calculated from the MMAT, perturbed by a sinusoidal function whose maximum and minimum
427 amplitudes are determined by mean monthly July and January temperatures, respectively. Daily
428 cumulative PDDs for each month are calculated using a probability function based on a relationship
429 between the standard deviation of daily to mean monthly temperature. Palaeo-climate forcing is
430 implemented from the 50-year interval NGRIP $\delta^{18}O$ record (Andersen et al., 2004), scaled between a
431 maximum prescribed temperature depression and present-day conditions. The inclusion of an
432 additional bulk offset within the temperature scaling calculation controls the degree of fluctuation
433 within the forcing record. Precipitation distributed evenly throughout the year, and accumulates as
434 snow when the surface temperature falls below a threshold of 1 °C. Winter expansion of sea ice
435 across the North Atlantic probably impacted upon precipitation seasonality during stadial conditions,
436 leading to a summer bias in the annual precipitation distribution across maritime sectors (Thomas et
437 al., 2008; Koenigk et al., 2009). Annual precipitation totals were thus likely greater than implied by
438 the effective precipitation volumes recorded by glacier geometries due to the expected increased
439 losses from the system associated with summer rainfall (Golledge et al., 2010).

440 Both temperature and precipitation adjust to the evolving ice-sheet surface (corrected for isostatic
441 loading) through applied lapse rates, derived from multiple-regression analyses of meteorological
442 observations over the reference period (1961-1990 provided by the Icelandic Meteorological Office)
443 (Björnsson et al., 2007; Crochet et al., 2007) (**Figure 3**A-C).

444 Independent variables used in the regression analysis for temperature include easting, northing, and
445 elevation. To determine the spatial pattern of the precipitation, an additional independent

parameter was used - δ_{temp} - the residual difference between the summer and winter temperatures, which provides a convenient proxy for "continentality". R^2 values of 90 % and 88 % give confidence that these three variables robustly account for the main temperature variability across the model domain. The R^2 for the present-day distribution of annual precipitation indicates a weaker correlation at c. 62% (Table S1). A limitation of the model is that we do not calculate the general circulation. Large-scale changes in climate related to shifts in atmospheric circulation are thus not accounted for, although broad scale distributions, for example rain shadow effects, can be incorporated manually by the application of linear gradients.

Mass wastage at tidewater margins is calculated according to the frontal calving geometry using an empirically derived depth-related algorithm (Brown et al., 1982). This calving parameterisation is not physically based but does, implicitly, account for the area of the tidewater front exposed to submarine melting – an important, significant yet under-represented component of mass loss from the termini and ice shelves of marine-ice sheets (e.g. Rignot et al., 2010; Nick et al., 2012; Chauché et al., 2014).

3.2. Topography

The model is applied to a finite-difference domain of 1300 x 650 km at 2000 m horizontal resolution encompassing the entire Icelandic continental shelf. Present-day onshore topography was extracted from digital elevation data sourced from http://www.viewfinderpanoramas.org/dem3.html with a resolution of 3 arc seconds (c. 90 m), and offshore bathymetry from the GEBCO_08 world data set at a resolution of 30 arc seconds. All topographic data were merged onto a Gall cylindrical equal-area projection, and a point grid used to extract the required elevation data in order of priority (**Figure 3**D).

3.3. Geothermal heat flux

Subsurface thermal gradients are dependent on four factors: 1) the regional heat flow through the crust, 2) hydrothermal activity, 3) permeability of the rock, and, 4) the residual heat build-up in extinct volcanic centres (Flóvenz and Sæmundsson, 1993). Given the strong influence of the active volcanic rift zone dissecting Iceland, background heat-flux values vary considerably from 80 to 310 mW m^{-2} across the domain. The pattern of geothermal heat flux used as a basal thermal boundary condition was determined from temperature measurements taken at the base of shallow (30-60 m) boreholes (Flóvenz and Sæmundsson, 1993) that are interpolated across the model domain using a standard kriging gridding algorithm with a linear variogram model containing no anisotropic weighting (**Figure 3**E).

4. Experiment results and selection

Although the model has a limited number of primary parameters (cf. Table 1), the uncertainty in model trajectory can be significantly reduced through sensible – empirically guided – parameter choices, and critical comparison of output with geological evidence. However, the challenge in accurately reconstructing the IIS is further compounded by the fact that extreme rates of mass-loss are possible across the marine-terminating margins through calving and submarine melting, introducing potential non-linear feedbacks within the climate–ice-sheet–ocean system. Onshore, the experimental problem is better defined, as here the first-order control on terrestrial ice masses is the spatial distribution of accumulation and ablation (cf. Hindmarsh, 1993). Hence, once offshore, marine ice-sheet dynamics add a level of system complexity regardless of climate forcing. Given the poor chronological constraints available for determining rates of ice-sheet advance and retreat (section 2), any reconstruction generated will remain symptomatically ambiguous.

Despite such uncertainties, broad thresholds for imposed climatic forcing can be identified through incremental iteration of the principal parameters. Furthermore, the optimal reference experiment singled out in this study constitutes a result considered to best represent and honour the most recent advances in our understanding of the extent and dynamics of the former ice sheet. Despite the disparate chronological and geomorphological constraints previously described (cf. section 2) (**Figure 1-2**), the reconstruction is glaciologically consistent and provides a basis for future refinement once further empirical constraints emerge. Key time-slices tracking the evolution of ice sheet extent and its associated flow dynamics are provided (**Figure 4**), with corresponding time-series of volume and area (**Figure 5**).

4.1. Reference experiment

A number of broad features within the reference experiment derived here are consistent with previous empirical and modelled IIS reconstructions: i) the broadly trending east-west orientated ice-divide centred over the northern margin of present-day Vatnajökull and its major dog-leg extension into Vestfirðir, ii) efficient drainage via numerous topographically constrained outlet glaciers that penetrate far into the interior of the ice sheet via the major fjord systems, and iii) a grounding-line well below LGM sea-level driving high rates of calving in marine-sectors.

The reference experiment requires a mean annual air temperature (MAAT) depression of at least 9.5°C from present day values over the duration of the LGM. Additional cooling beyond this threshold has little impact on the ice sheet reaching its maximum extent at the shelf edge, with precipitation rates becoming the key climatic variable for determining the pace of ice build-up and total volume.

However, there are numerous and significant differences between the reference experiment presented here and that of Hubbard et al. (2006) most notably in terms of ice sheet advance and

extent to the continental shelf edge. Whereas the reconstruction of Hubbard (2006) actively limited ice development on the Langanes Peninsula and the northern shelf through the imposition of strong precipitation gradients, here ice expansion to the north, east and west of Iceland is unhampered (**Figure 4**). Precipitation rates in our reference experiment are reduced across the whole domain during the LGM by 40%, with a positive west to east gradient of 35 % imposed from 17.53°W. Moreover, whereas Hubbard (2006) initiates the LGM experiments at 24 ka BP with a 5°C cooling and terminates them at 21 ka BP; experiments here are initiated at 35 ka BP and are forward integrated until 10 ka BP. The increased model time-span enables the ice-sheet to initiate and its climate and flow dynamics to physically and numerically stabilise and relax completely to the imposed forcing.

The ice sheet's relatively simple form and large, central ice divide mean that growth and retreat of the ice sheet is largely radially symmetrical across marine sectors. Exceptions are along the southern coast where the narrow width of the continental shelf acts as a natural topographic barrier to ice sheet growth. Ice flow is relatively stable throughout the maximum configuration with large sectors of the ice sheet bed consistently at pressure-melting point (**Figure 6**A), resulting in stable patterns of basal motion and fast-flow drainage throughout. The absence of strong ice-stream switching throughout this maximal configuration, as has been suggested for other palaeo ice sheets (MacAyeal, 1993; cf. Hubbard et al., 2009; Stokes et al., 2016), yields stable margins offshore for almost 2,000 yr during the LGM (**Figure 7**).

The modelled LGM ice sheet has a maximum total area of 5.62 x 10^5 km^2 and a concomitant volume of 6.58 x 10^5 km^3 - a two-fold increase on both metrics compared to the reconstruction by Hubbard et al. (2006) - and equates to a net eustatic contribution of c. 1.53 m of global sea-level equivalent. For ice grounded below sea-level, the net mass contribution to sea-level rise was taken from ice lying between the flotation level and the ice surface, calculated assuming an ice density of 917 kg m^{-3} and sea-water density of 1030 kg m^{-3}. Mean LGM ice-thickness is just over 1,172 m, 233 m greater

543 than that previously reconstructed by Hubbard et al. (2006) (Table 3). The modelled ice-sheet
544 surface rises to an elevation of c. 1850-1900 m along the central drainage divide, attaining a
545 maximum surface height of 2093 m around Öræfajökull, south of Vatnajökull.

546

547 ## 4.2. Ice-sheet sensitivity

548 The LGM reference experiment was subject to a series of sensitivity experiments that explored, in
549 turn, the broad influence of individual parameters on ice sheet form and flow. The following
550 parameters and variables are explored: sea-level forcing; sensitivity to calving; sensitivity to sliding;
551 geothermal heat flux along with initial ice-sheet geometry (Table 3).

552 ### 4.2.1. Inherited ice-sheet geometry

553 Given the limited availability of empirical data relating to Icelandic glaciation during MIS3, two
554 experiments were conducted to explore the influence of inherited ice-sheet geometry prior to the
555 'LGM' timeframe (26.5 - 19 ka: Clark et al., 2009). To achieve this the MAAT forcing curve was shifted
556 ±2°C from the reference experiment with imposed precipitation patterns left unchanged.

557 Despite very contrasting geometric trajectories during initial build-up, the two resulting ice sheets
558 closely match the dimensions of the reference experiment at the peak of the LGM, with areal and
559 volume differences of ≤3 % (Table 3). With the same deglaciation forcings, the ice sheet aligns once
560 more with the mass loss trajectories originally calculated in the reference experiment, revealing that
561 once the ice sheet reaches the shelf break in all sectors a state of equilibrium with the forcing
562 climate appears to be quickly reached.

563 ### 4.2.2. Sea level and ice calving

564 Calving has a primary role in the stability of tidewater glaciers and marine ice sheets (Rott et al.,
565 2002; Rignot and Kanagaratnam, 2006; Howat et al., 2007; Rignot et al., 2010). Model sensitivity to
566 calving is thus explored through large-scale perturbations of the calving parameter (*C*) and also

567 through rescaling of the eustatic forcing curve by ±50 m. Reduction of sea level by a further 50 m
568 yields a slightly larger ice sheet (2.9 %) than the reference experiment. Conversely, an increase of
569 sea levels by 50 m leads to increased calving front losses and a restricted ice sheet that is reduced in
570 volume by 15 % at the LGM. Although the ice sheet still inundates the majority of the Icelandic
571 continental shelf, the mass losses at the ice margin influence ice thickness, with a concomitant ice
572 surface lowering of c. 4 %.

573 Order-of-magnitude changes in the calving parameter have a dramatic effect on the modelled ice
574 sheet. Increasing the calving parameter yields an ice sheet that is almost exclusively terrestrially
575 based, with corresponding volume and area reductions of 29 % and 22 % respectively. Conversely, a
576 lowered calving parameter value produces significant increases in area and volume by 17 % on the
577 reference experiment. However, ice expansion is limited primarily by the offshore bathymetry, since
578 beyond the continental shelf-edge the sea-floor is too deep for ice to remain grounded.
579 Furthermore, decreased sensitivity to calving leads to a slight net thinning of the ice sheet at its
580 maximal configuration, driven by ice-sheet expansion into marine sectors that are below the
581 equilibrium line, and thus more susceptible to surface melt processes – a somewhat counter-
582 intuitive result.

583 #### 4.2.3. Sliding versus internal deformation

584 Whilst mass balance is the first-order control on ice-sheet growth and decay, ice-flow regime
585 determines the response, sensitivity, and overall ice sheet geometry (i.e., aspect ratio, volume and
586 hypsometry) particularly across marine sectors. Importantly, the partitioning of basal motion within
587 the ice-sheet model is linked to geothermal flux and melting at the ice-bed interface. Experiments
588 were thus conducted to explore the degree to which basal motion is critical to ice-sheet stability and
589 response time, and how altering the effective viscosity affects the ice sheet's ability to transport
590 mass from the interior to the margin. Where basal sliding occurs, its effectiveness is linked to bed
591 roughness; thus the higher the sliding parameter value, the easier ice can flow over obstacles at the

bed. Two experiments with order-of-magnitude change in the sliding parameter (A_{weert}) were conducted.

A reduction of A_{weert} yields a stiffer (increased viscosity), thicker, less extensive ice sheet which has much less mobility. Consequently, the ice sheet is less sensitive to external climatic forcing with a supressed response and dampened fluctuations in lateral extent. In contrast, increasing A_{weert} by an order of magnitude facilitates greater mobility and lateral expansion of the ice sheet through increased flow, and results in a lower aspect ratio and mean ice thickness relative to the reference experiment. The main impact of increased basal motion is increased sensitivity of a lower aspect ice sheet to rapid fluctuations, particularly during deglaciation through accelerated flow and draw-down of interior ice to the margins where surface melting, calving processes and the associated dynamic feedbacks dominate.

4.2.4. Geothermal forcing

Changes in geothermal heat flux impact on modelled ice-sheet flow dynamics through their effect on the zonation of subglacial thermal conditions (warm/temperate vs. cold/frozen) and hence the distribution of basal motion. Four experiments examining the influence of the geothermal boundary condition are conducted, using the following scaling values of the present-day geographical distribution of geothermal heat flux: 1.5, 0.5, 0.25 and 0.1.

Increasing the present-day geothermal heat flux throughout the experiment causes negligible dimensional change to the ice sheet (Table 3). The natural topographic barrier of the continental shelf edge prevents any further significant expansion, and with an already low surface-aspect ratio in the reference experiment, ice-sheet volume and thickness remain unchanged. Slight differences are more apparent under geothermal flux reductions. Changes in ice sheet areal extent are generally small, though values of maximum volume, and consequently mean thickness, tend to increase. Under 10% scaling of the geothermal heat flux (range: 7-31 mW m^{-2}), the ice sheet mobility is

reduced resulting in a 4 % increase in volume, and 5 % thicker ice sheet than the reference experiment.

Critically, changes in the geothermal heat flow to the ice-sheet bed has a significant impact on its flow and drainage properties (**Figure 7**). Under the relatively warm geothermal conditions of the present-day geothermal flux (Figure 2E) the ice sheet experiences constant basal melting, thereby promoting stable and continuous fast-flow drainage and a relatively shallow ice-surface gradient. Increases to the geothermal flux provide negligible changes, though by coupling a basal hydrological system to the model further insights may be gained in this respect.. Conversely, with decreased geothermal heating forcing, the spread of extensive cold-based ice induces dynamic instabilities, causing rapid and dramatic switches in basal motion once basal conditions attain pressure melting point during periods of climate amelioration. These flow cycles are increasingly vigorous when the ice sheet is thinnest during the first 10 ka of ice build-up, with dramatic switching in ice discharge varying by a factor of 4-5 on centennial timescales.

When geothermal fluxes are modified to values more closely aligned with background continental fluxes (0.25G: 17-77 mW m^{-2}), the coverage of areas that could potentially host cold-based ice become evident. If the present-day ice caps are ignored, where it has not been possible to incorporate subglacial topographies, cold-based areas are abundant among the high relief of the south-eastern and eastern fjords, the Tröllaskagi Highlands, and to a lesser extent the Vestfirðir peninsula (Figure 6). For the latter, the pronounced geothermal hotspot across Snæfellsnes keeps basal conditions persistently warm on this peninsula, particularly in the east (Figure 3E; Flóvenz and Sæmundsson, 1993).

5. Discussion

5.1. Ice-flow directions and ice limits

Pre-LGM radiocarbon dates from Reykjanesskagi, which at this time would have been within the sub-aerially exposed Faxaflói indicate that the ice sheet probably traversed this peninsula c. 28 cal. ka BP (**Figure 1**A). From an initial ice-free domain, the modelled ice sheet is able to reach this coastline position within 7 ka of glaciation, expanding rapidly in response to strong precipitation input and the coalescence of five major ice nucleation centres over the four present-day ice caps and the Tröllaskagi Highlands. Limited relief over Vestfirðir leads to more subdued ice growth here that eventually becomes engulfed by the mainland ice sheet c. 29 ka BP. The close proximity of the southern shelf edge means the maximum ice-sheet extent in this sector is reached considerably early during the glaciation at c. 29 cal. ka BP. Elsewhere, the last terrestrial areas of Iceland to be overrun by ice include the tips of the Langanes, Vestfirðir (Látrabjarg) and Snæfellsnes peninsulas at 27.8 ka BP.

Growth of the modelled ice sheet continues synchronously up to the continental shelf edge to the north, east and west, reaching this position in all sectors by c. 23.7 ka BP. Here the IIS remains stable for the next 2 ka, reaching an absolute maximum extent at 22.9 ka BP, with significant retreat initiating after c. 21.8 ka BP. The total contribution to global eustatic sea-level rise at this time reaches a maximum value of 1.53 m

The symmetric nature of the ice sheet, as well its radial ice-discharge pattern, results in a very stable central ice divide that undergoes little migration throughout the entire glaciation. Isostatic deepening of the offshore troughs, coupled with the short isostatic response time of the crust (Sigmundsson, 1991), further stabilises the pattern of ice drawdown from the interior of the ice sheet into marine-based corridors.

660 Glacial lineations are a common landform signature of palaeo-ice sheets, indicative of fast, ice-
661 streaming flow (Clark, 1993; Ó Cofaigh et al., 2002; Stokes and Clark, 2002; King et al., 2009), and
662 have been readily identified across the Icelandic shelf to infer the presence of numerous ice streams
663 that drained ice towards the shelf edge and an ice divide across central Iceland from east to west
664 (Bourgeois et al., 2000; Stokes and Clark, 2001; Spagnolo and Clark, 2009; Principato et al., 2016).
665 These flow sets mapped from Landsat satellite imagery and the Olex bathymetry database (**Figure 2**)
666 reveal a good correspondence both on- and offshore (**Figure 8**), supporting the radial form and
667 detailed flow pattern of the reference model experiment presented here. Closer analysis of
668 modelled vectors reveals a pattern of flow adjustments through the latter stages of deglaciation. For
669 example, ice flow towards Húnaflói and Héradsflói (sector 1 & 4 – **Figure 8**) both show an increased
670 correspondence with the geomorphological record during the last major readvance of the ice sheet
671 in the Younger Dryas. Such subtle variations in ice-sheet flow are typical of internal reconfigurations
672 during ice-sheet thinning as ice divides adjust in response to the increasing influence of bed
673 topography, though may also be a reflection of the greater abundance of empirical data reported
674 onshore.

675 ## 5.2. Ice-sheet collapse

676 At the LGM, 60% of the IIS was grounded below sea level, of which two-thirds (40% of the IIS) was
677 grounded in water depths greater than 100 m (**Figure 4**). In terms of net contributions to global sea
678 level, c. 53 % of the total 1.5 m s.l.e. of the maximum IIS came from grounded ice with a bed below
679 sea level. Compared to ice cover over West Antarctica, the only present-day marine-based ice sheet,
680 this contribution is much higher at 79 % (Fretwell et al., 2013). In both instances, these values
681 highlight the sensitivity of both marine-based ice sheets to external fluctuations in oceanographic
682 forcings such as sea-level or ocean temperature.

683 Limited dating suggests retreat of the IIS from the shelf was rapid, probably largely forced by
684 oceanographic drivers including rising sea-level and the northwards migration of the Polar Front

(Ingólfsson and Norðdahl, 1994, 2001; Andrews et al., 2000; Eiríksson et al., 2000; Jennings et al., 2000; Geirsdóttir et al., 2002; Andrews, 2005, 2008; Norðdahl and Ingólfsson, 2015). The general absence of submarine recessional-moraine sequences has been used to support this hypothesis, though with few clear offshore topographic pinning points, deglaciation was probably predisposed to unstable retreat (e.g. Dyke, 2004). The northwest sector (Vestfirðir) presents the single exception to this generalised pattern, where several nested suites of large offshore moraines record local grounded still-stands and/or readvances (**Figure 2**).

Surface-exposure (^{36}Cl) dating of bedrock and boulders from Vestfirðir suggests that the ice sheet was thinning across the uplands here as early as 26.2 ka BP (Brynjólfsson et al., 2015). Although the reference experiment fails to reproduce this early thinning necessary to expose nunataks on the Vestfirðir peninsula, the absolute elevation of the ice surface was lowering from c. 24 ka BP in response to the propagating isostatic depression of the crust. The isostatic response to ice-sheet loading could therefore provide a mechanism by which nunataks emerge early above the ice-sheet. Through rapid depression of the interior sectors of the ice sheet, the relative shift of the equilibrium-line altitude up-glacier would subsequently expose far greater areas of the ice sheet to ablation processes, potentially prior to any external climatic forcing.

From the maximal configuration at c. 21.8 ka BP, deglaciation occurs in two phases with distinctly different styles. While initial instability is triggered by abrupt climate warming, subsequent retreat ensues through disproportionate losses from calving (c. 45 % of total losses; Table 4; **Figure 9**). Modelled ice retreat from the shelf edge to the present-day coastline is accomplished within 3.8 ka along eastern sectors, and 5.0 ka in the west; the longer timeframe in accordance with the presence of potential recessional moraines on the shelf in this sector, and possibly sustained by the topographic influence of Vestfirðir nearby. The volumetric loss is significant, with average mass wastage rates of c. 71 Gt a^{-1} between 21.8 ka BP to 18.0 ka BP - equating to a mean eustatic sea-level contribution of 0.196 mm a^{-1}. For context, contemporary mass balance estimates for the West

710 Antarctic ice sheet and the Greenland ice sheet have been recently estimated at -102±18 and -
711 263±30 Gt a^{-1} respectively (Shepherd et al., 2012; Hanna et al., 2013). For the IIS, an ice sheet with a
712 maximum volume less than a third of the present West Antarctic Ice Sheet (Fretwell et al., 2013),
713 the implication is that once deglaciation initiated it was extremely rapid.

714 As climate amelioration continues and the ice sheet becomes progressively terrestrial based, a
715 switch in deglaciation style occurs, whereby surface melting begins to dominate the mass balance
716 regime. Topographic pinning points between the island's peninsulas halt the rapid retreat of the ice
717 sheet from the outer shelf at 16.3 ka BP, holding the ice margin in place until further abrupt warming
718 during the Bølling interstadial at 14.9 ka BP initiates a second ice-sheet-wide collapse. This phase of
719 rapid deglaciation is a common feature to all model experiments (**Figure 5**), with mass losses
720 occurring at a mean rate of 221 Gt a^{-1} over 740 years (melt >91 % of total losses; Table 4; **Figure 9**),
721 and resulting in a Late Weichselian minimum extent of 0.986 x 10^5 km^2 shortly after at 13.2 ka BP
722 (**Figure 4**).

723 A similar-style ice-sheet collapse event on the inner Icelandic shelf within a few centuries has been
724 inferred based on radiocarbon dates of c. 15.0 cal. ka BP in Jökuldjúp and 14.8 cal. ka BP from the
725 150 m high marine limit at Stóri-Sandhóll, west Iceland (Jennings et al., 2000; Ingólfsson and
726 Norðdahl, 2001; Principato et al., 2005) (**Figure 1**B). Various factors have been suggested to account
727 for this dramatic 125 km retreat inland, including a contemporaneous and rapid eustatic sea-level
728 rise during MWP-1A, in combination with a short-lived temporal equilibrium between glacio-isostatic
729 uplift and sea-level rise (Norðdahl and Ingólfsson, 2015). While the marine-terminating ice sheet
730 would have undoubtedly been sensitive to rapid fluctuations in oceanic forcings, the model clearly
731 relates rapid retreat at this time to atmospheric warming significantly elevating the equilibrium-line
732 altitude. The surface area of the ablation zone across the ice sheet rises from 35% to 83% in just 500
733 years (**Figure 10**), this dynamic further intensified by the rapidly responding isostatic rebound of the
734 crust at this time.

735 The isostatic adjustment scheme coupled to the ice-sheet model (in this study) predicts that the
736 greatest depression during the LGM probably occurred over northwest Iceland. This area coincides
737 with the areas of greatest ice thicknesses at the LGM, in the major topographic lows of Breiðafjörður
738 and Húnaflói close to the central ice divide (**Figure 11**). Isostatic adjustment values at this time
739 equate to c. 200 m depression below the present-day level, far from the 570 m of depression
740 predicted by Norðdahl & Ingólfsson (2015) at the present-day coastline using steady-state equations.
741 Further discrepancies in southern Iceland between the position of the modelled coastline and the
742 marine ice-contact deltas found in the Búði moraine complex at the time of the Younger Dryas
743 (**Figure 12**) (Geirsdóttir et al., 1997) indicate that isostatic depression is underestimated within the
744 reference experiment. Considering uplift rates during deglaciation reached as high as 107 mm a^{-1}
745 (Rundgren et al., 1997), the acute sensitivity and heterogeneity of crustal deformation around
746 Iceland makes this a clear challenge for ice-coupled modelling. Accurate reconstruction of relative
747 sea-level curves and uplift rates would therefore be best resolved through explicit Glacial Isostatic
748 Adjustment (GIA) modelling, whereby independent predictions of ice thickness can be incorporated
749 to explore the full range of viable Earth rheology parameters (e.g., Auriac et al., 2013).

750 ## 5.3. Ice sheet aspect ratio

751 The collection of numerous cosmogenic-exposure age dates from table mountains within the
752 neovolcanic zone (Licciardi et al., 2007) provides valuable constraints with which to reconstruct the
753 surface-aspect ratio and slope of the retreating ice sheet. While these dates are limited to two
754 discrete time intervals during deglaciation related to episodes of high volcanic activity (c. 14.4 - 14.2
755 ka and 11.1 - 10.5 ka), the data consistently predict a low aspect-ratio ice-sheet surface with slope
756 gradients between 1:125 and 1:180. The geometry of the reference modelled ice sheet presented
757 here reproduces similar shallow surface gradients of between 1:172 and 1:192 during deglaciation
758 (**Figure 13**) providing verification that the mass-balance and flow regime are broadly correct and
759 consistent.

North of Vatnajökull, during the Bølling climatic oscillation at 14.7 ka BP, the modelled ice sheet overruns the isostatically adjusted table mountain summits of Bláfjall and Gæsafjöll by c. 400 m, more than the 15 % of the total thickness as suggested by Smellie (2000) necessary for their subglacial formation. The modelled ice sheet margin falls 10 km short of Snartarstaðarnúpur, though the low elevation of this mountain indicates that ice cover was probably not particularly thick here when it last erupted. Differences southwest of Langjökull are more pronounced due, in part, to conflicting interpretations of the extent and form of the Younger Dryas ice sheet. The reference model extent was largely constrained in this sector by the large Búði moraine complex (**Figure 1**) (Geirsdóttir et al., 1997, 2000). Dated table mountain summits outside of this limit (e.g. Geitafell and Hvalfell), contradict this interpretation, indicating that ice extent was possibly much greater at this time. On discussion of their samples, Licciardi et al. (2007) noted that any snow or rime-ice shielding over the mountain summits could increase the reported ages by up to 18%. Though this may not be sufficient to account for differences in the modelled ice extent, it raises the possibility that mountains near the margin of the ice sheet may have hosted persistent and independent ice fields during the Younger Dryas stadial.

Modelled ice surface slopes are even shallower within the ice-sheet interior during the maximal configuration (> 1:208), comparable with slope measurements from the present-day Greenland and Antarctic ice sheets (cf. Bamber et al., 2013; Fretwell et al., 2013). Despite this, the modelled Icelandic ice sheet is still sufficiently thick to override previously assumed nunataks, such as in the Tröllaskagi highlands (Norðdahl, 1983), and on Vestfirðir and Skagi (Principato and Johnson, 2009). Based on palaeo-analogues in other glaciated regions (e.g. Ballantyne, 2010; Fabel et al., 2012), the assumption that the erosional (trimline) boundaries mapped in Iceland represent palaeo-ice surfaces is worthy of re-examination in the context of the shelf-edge glaciation model presented here.

5.4. The Younger Dryas

The reference model experiment of the Younger Dryas Stadial presented is in good agreement with leading interpretations from the empirical record, with ice margins restricted largely to the present-day terrestrial landmass (**Figure 12**). Truncated raised marine shorelines in the mouths of fjords and major valleys around Iceland demonstrate that the Younger Dryas ice sheet expanded across many coastal sites that had been ice-free since the Bølling deglaciation (~14 cal. ka BP) (cf. Ingólfsson et al., 2010). For example, large outlet glaciers filled the largest northern fjords of Skagafjörður, Eyjafjörður and Skjálfandi (Norðdahl and Haflidason, 1992; Norðdahl and Pétursson, 2005), draining ice from the main central ice-divide. However, occurrences of the Skógar-Vedde tephra in ice-dammed lake sediments in Fnjóskadalur show that numerous ice-free enclaves existed in north central Iceland at this time (Norðdahl and Haflidason, 1992). This evidence indicates that the modelled ice sheet reconstruction could be generally too thick in this sector. Furthermore, truncated shorelines on the Langanes Peninsula also reveal that only the easternmost part of the peninsula was probably ice-free during the YD (Pétursson, 1991; Norðdahl and Hjort, 1995). However, model experiments consistently fail to glaciate this northeastern sector due to the long distance from the nearest accumulation centre around present-day Vatnajökull.

Northeast of Reykjavík at Helgafellsmelar, the termination of the Younger Dryas glacial advance is marked by ice-contact deltas and related shoreline features radiocarbon dated to 11.8 cal. ka BP (Ingólfsson et al., 1995). However, this position is difficult to reconcile with an apparent Younger Dryas ice limit also constrained by the Búði moraine complex ~100 km to the east (cf. Norðdahl et al., 2008). In light of this evidence, it is probable that local (semi) independent ice fields persisted on the higher terrain of Reykjanesskagi throughout the Younger Dryas stadial (e.g., Geirsdóttir and Eiriksson, 1994).

5.5. Geothermal forcing

A major question regarding the LGM configuration is the extent of ice cover on Vestfirðir and its association with the mainland ice sheet. Geomorphological features such as preserved upland block-fields, arêtes and old ^{36}Cl dates have been used to infer the presence of extensive cold-based ice or minimal glacial erosion here during the LGM (Principato et al., 2006; Brynjólfsson et al., 2015). Model experiments presented here appear to contradict the empirical record in this respect due to the effect of the large geothermal fluxes recorded from eastern Vestfirðir encouraging permanent subglacial melt in this sector (Figure 3E; Flóvenz and Sæmundsson, 1993). By reducing the geothermal flux to nearer background continental values, basal thermal partitioning does indeed become more pronounced, with upland areas remaining frozen for up to 45% longer during glaciation (**Figure 6**). Given the sensitive nature of the ice sheet to the geothermal boundary condition, it appears further data concerning the heterogeneous distribution of the geothermal flux across Iceland are necessary before accurate modelling of the basal thermal regime can be achieved.

At the broad scale, model experiments confirm that geothermal heat gradients can exert a primary influence on ice sheet sensitivity and dynamic response. For the IIS, increased geothermal heat supply to the ice-bed interface plays a minor role on ice growth trajectories (Table 3), which is ultimately restricted by the continental shelf edge. However, it is reductions in geothermal forcing to values closer to those measured over ancient continental shields that lead to the most notable changes in its behaviour.

The predominant response is the shift from persistent pressure melting induced at the base of the ice sheet to a cyclical phasing of ice-stream shutdown and reactivation on sub-millennial timescales (**Figure 6,**

Figure 7). The timing and dynamics of these flow-phasing events are determined through a combination of basal thermomechanical switching spatially propagated and amplified through longitudinal coupling. However, it is the major oscillations within the NGRIP climatic record used to

831 force the model that modulate the main phases of streaming activity. Relatively thin ice-sheet outlet
832 glaciers, particularly those terminating in marine sectors, are most sensitive to these changes where
833 advection of warmer ice through the ice-mass is rapidly achieved, inducing basal melting and
834 subsequent fast-flow. Such dynamic behaviour resonates with other modelling studies showing that
835 basal ice temperatures are highly sensitive to relatively small changes in geothermal heat flow
836 (Greve and Hutter, 1995; Siegert and Dowdeswell, 1996; Tarasov and Peltier, 2003; Greve, 2005).

837 In previous studies where spatially varying geothermal heat-flow distributions have been used,
838 modelled ice-sheet reconstructions have shown significant sensitivity and variation (e.g. Näslund et
839 al., 2005; Rogozhina et al., 2012). For palaeo-ice sheets where geothermal heat flow is relatively
840 heterogeneous, or dominated by relatively low continental flux values, the implication for transient
841 dynamic behaviour is significant. Examples include the eastern Laurentide and northern
842 Fennoscandian ice sheet sectors, flowing over bedrock largely composed of Caledonian-age
843 crystalline lithologies. Borehole measurements in these regions have revealed low geothermal heat
844 fluxes of < 34 mW m^{-2} (Lubimova et al., 1972; Kukkonen, 1989; Rolandone et al., 2003). The
845 increased sensitivity of the ice sheet to thermal conditions at the ice-bed interface partly explains
846 the resulting unstable dynamics, or ice-stream purges, that have been inferred for these sectors
847 during deglaciation under a rapidly changing climate (e.g. MacAyeal, 1993; Papa et al., 2005;
848 Winsborrow et al., 2010). Moreover, geothermal hotspots have been identified beneath the current
849 Polar ice sheets, including the Northeast Greenland ice stream (Fahnestock et al., 2001), and the
850 Siple Coast, West Antarctica (Engelhardt, 2004; Winberry and Anandakrishnan, 2004; Corr and
851 Vaughan, 2008), where the first direct measurement of geothermal heat flux has been recorded at
852 285 ± 80 mW m^{-2} beneath the Whillans ice stream (Fisher et al., 2015) – comparable with the upper
853 range of fluxes within the current Icelandic neovolcanic zone. The implications of our findings for ice-
854 stream stability and rapid ice sheet drawdown are thus significant for determining scenarios of
855 future non-linear deglaciation.

6. Conclusions

- Limited empirical data from a variety of sources indicate that an extensive marine-based ice sheet occupied the Icelandic continental shelf between 28.1 – 15.4 cal. ka BP. Although chronological constraints are poorly distributed, the offshore glacial geomorphological footprint described here indicates that the Icelandic ice sheet probably reached the continental shelf edge in all sectors during the Last Glacial Maximum before rapidly collapsing.
- In this paper we incorporate coupled climate-flow modelling to examine this concept of a shelf-wide Late Weichselian Icelandic Ice Sheet within the context of available empirical constraints, providing a robust reconstruction that describes the growth and subsequent deglaciation trajectory through to the Younger Dryas and Early Holocene.
- The maximum areal extent of the reference ice sheet is almost double the previous reconstruction by Hubbard et al. (2006) at 5.62 x 10^5 km^2. Due to the primary influence of geothermal heat supply on the dynamics of the Icelandic ice sheet, a low aspect ratio is maintained with a mean thickness of 1172 m and volume of 6.58 x 10^5 km^3 at the LGM, equivalent to 1.53 m of eustatic sea level.
- At the LGM, 60 % of the Icelandic ice sheet was grounded below sea-level, bounded across all sectors by an active calving margin that extended to the continental shelf break. During subsequent deglaciation the retreat rate of this marine-based ice sheet was rapid, losing mass at a mean rate of 71 Gt a^{-1} between 21.8 and 18.0 cal. ka BP.
- Once pinned on the present-day coastline, the ice sheet underwent a second more abrupt phase of collapse at the start of the Bølling-Allerød interstadial (GI-1e), losing mass at a mean rate of 221 Gt a^{-1} over the course of c. 750 years, forcing retreat of the ice sheet firmly into terrestrial sectors. The bulk of mass loss during this period comes from surface melt in

response to climate warming, forcing a widespread increase in the elevation of the equilibrium-line altitude and exacerbated by the already low aspect-ratio of the ice surface.

- While the areal extent of the ice sheet has a strong topographic control, ice thickness and volume respond dramatically to long-term changes in the basal thermal regime, and consequently the effective mobility of the ice sheet. Reduced geothermal heat flow to the ice-bed interface increases the sensitivity of marginal sectors to cycles of centennial-scale fast-flow conditions. These are in turn are modulated by transitions from cold to warm phases of the NGRIP temperature forcing curve.
- The major influence that basal geothermal heat supply imparts on ice-sheet flow dynamics suggests that further work is required to explore the role of this transient boundary condition. Adopting a fully coupled ice-lithosphere-mantle model, in addition to the introduction of a subglacial hydrology layer, would provide further insight into the behaviour, evolution and feedbacks between ice sheets and their geothermally active beds.

Acknowledgements

The initial modelling work was supported by a Joint Studentship (2K08/E108) provided by the British Geological Survey and Aberystwyth University via the BGS-University Funding Initiative and from the Climate Change Consortium of Wales (C3W). HP and AH also gratefully acknowledge support from the Research Council of Norway through its Centres of Excellence funding scheme, project number 223259, and the PetroMaks project “Glaciations in the Barents Sea area (GlaciBar)”, project number 200672. Echo-sounder bathymetry data products have been derived from the EMODnet Bathymetry portal - http://www.emodnet-bathymetry.eu. Two anonymous reviewers are thanked for their constructive comments.

Figure captions

Figure 1: A) Suggested limits of the last Icelandic Ice Sheet based on geophysical data observations, alongside radiocarbon dates (cal. ka BP) constraining an upper age for Late Weichselian glacier expansion (red) and radiocarbon dates from probable reworked sediments (yellow) (cf. Table 1). B) Key radiocarbon dates constraining deglaciation of the Late Weichselian ice sheet, alongside the speculated limits of the Younger Dryas glacier expansion (Pétursson et al., 2015). The present-day neovolcanic zone is characterised by relatively high geothermal heat fluxes and volcanic eruptions, forming part of the active Mid-Atlantic lithosphere boundary.

Figure 2: A) Overview of the glacial geomorphology of the Iceland continental shelf (Spagnolo and Clark, 2009), corroborated and supplemented with additional landform mapping from Landsat satellite imagery (onshore) and the EMODnet DTM (offshore – dark colours). Increased bathymetry data coverage to the northwest in particular reveal a number of newly identified glacial landforms close to the shelf edge. Trough extents are delimited as local topographic lows relative to the surrounding terrain. Flow sets onshore are grouped according to flow direction affinity and contiguity. B) Bathymetric profile over a prominent moraine ridge close to the northern shelf edge.

Figure 3: Model boundary conditions, climatic values derived from multiple regression analysis in Table 2. A) Mean January temperature, B) Mean July temperature, C) Mean annual precipitation, D) Melded topographic datasets, E) Geothermal heat flux - circle radii are scaled to the geothermal flux from each borehole, and F) Names and locations of the present day ice caps across Iceland. The blue arrow indicates the starting longitude and direction of the positive west-east precipitation gradient applied within the reference experiment.

Figure 4: Selected time slices showing surface-ice velocities between 31.0 and 11.7 ka BP from the reference model experiment. Compared to the reconstruction of Hubbard et al. (2006 shown in light blue, maximum expansion to the north, east and west is evident during the LGM.

Figure 5: Areal and volumetric sensitivity of the optimal experiment to magnitude changes in model parameter values. Abbreviations: A_{weert} (sensitivity to sliding), C (sensitivity to calving), SL (relative sea level), and T (mean annual air temperature prior to 28.5 ka BP).

Figure 6: Spatial partitioning of basal temperatures through the Late Weichselian glacial cycle under various geothermal flux scenarios. Dark green areas are more likely to be warm based throughout the glaciation, while purple regions more likely to be cold based. Regions beneath the present-day ice caps are masked, as data relating to their subglacial topographies were not included in the ice flow model and therefore basal conditions here are not calculated accurately.

Figure 7: The effects of scaled present-day geothermal forcing on the mean basal velocity of the ice sheet through the last glacial cycle. Centennial-scale thermomechanical switching, modulated by transitions in the climate forcing from relatively warm to cold conditions, become more apparent with reductions in the supply of heat to the base of the ice sheet. Increases beyond the present-day geothermal flux have negligible effects on the mean basal velocity regime.

Figure 8: Modelled basal velocity vectors (red) versus observed orientations of mapped glacial lineations (blue) on- and offshore during various stages of modelled ice retreat at 22.9, 14.7 and 11.7

ka BP. Notable examples of improved flow correspondence through deglaciation include group i offshore, and flow sets 1 and 4 onshore.

Figure 9: Mass turnover (Gt a^{-1}) and volume changes of the modelled Icelandic Ice Sheet through the Late Weichselian. Two periods of intensive deglaciation post-LGM are indicated, with greatest mass losses occurring during the climate warming of the Lateglacial interstadial. Greenland Interstadials are defined by the INTIMATE event stratigraphy (Rasmussen et al., 2014), and climate forcing applied through a scaled version of the NGRIP ice-core record (Section 3.1) (Andersen et al., 2004).

Figure 10: A) Changes in the proportion of the ice surface experiencing surface melting over a period of 500 years, leading to rapid retreat of the ice sheet during the Lateglacial interstadial; B-C) Sharp rises in the mean annual air temperature at this time led to more intensive surface melting at the ice sheet margins.

Figure 11: Ice thicknesses at the Last Glacial Maximum, showing thickest ice cover over the Breiðafjörður and Húnaflói. Present-day topography above 1 km a.s.l. (including the present-day ice caps) is indicated in black.

Figure 12: Surface velocities of the modelled Younger Dryas ice sheet, with the contemporary coastline calculated from isostatically adjusted topography. The ice sheet at this time reached a maximum elevation of c. 1750 m a.s.l. Speculated empirical limits for glacial extent at this time (black line) are shown for comparison (Pétursson et al., 2015).

Figure 13: Transects through the neovolcanic zone (inset – red) indicating locations of cosmogenic-exposure dated table mountains and modelled ice-sheet profiles from the reference experiment through deglaciation. Dated table mountains from Licciardi et al. (2007) include: (Bl) Bláfjall, (Bú) Búrfell, (Gæ) Gæsafjöll, (Ge) Geitafell, (Ha) Hafrafell, (He) Herðubreið, (Hö) Högnhöfði, (Hv) Hvalfell, (R) Rauðafell, (Sk) Skriða, and (Sn) Snartarstaðarnúpur.

Table captions

Table 1: Reported ^{14}C ages were recalibrated (unless starred) using the program Calib 7.1 (Stuiver and Reimer, 1993) and the IntCal13/MARINE13 calibration curves (Reimer et al., 2013). A ΔR value of 24±23 was used to account for local effects on the global reservoir correction (Håkansson, 1983).

Table 2: Principal parameters, constants and values used to force the ice-sheet model.

Table 3: Sensitivity of the reference experiment to magnitude changes of model parameters that control ice flow, calving, sea-level forcing and the basal geothermal heat flux. Variations in the MAAT climate forcing are shifted prior to 28.5 ka BP to influence the pre-LGM size of the ice sheet. Scaled variations of G are based upon the present-day distribution (including the neovolcanic zones). Ice volume, area, thickness values are taken from the maximal ice-sheet timeslice.

Table 4: Principal components of mass loss post LGM.

References

Andersen, K.K., Azuma, N., Barnola, J.-M., Bigler, M., Biscaye, P., Caillon, N., Chappellaz, J., Clausen, H.B., Dahl-Jensen, D., Fischer, H., Flückiger, J., Fritzsche, D., Fujii, Y., Goto-Azuma, K., Grønvold, K., Gundestrup, N.S., Hansson, M., Huber, C., Hvidberg, C.S., Johnsen, S.J., Jonsell, U., Jouzel, J., Kipfstuhl, S., Landais, A., Leuenberger, M., Lorrain, R., Masson-Delmotte, V., Miller, H., Motoyama, H., Narita, H., Popp, T., Rasmussen, S.O., Raynaud, D., Rothlisberger, R., Ruth, U., Samyn, D., Schwander, J., Shoji, H., Siggard-Andersen, M.-L., Steffensen, J.P., Stocker, T., Sveinbjörnsdóttir, a E., Svensson, A., Takata, M., Tison, J.-L., Thorsteinsson, T., Watanabe, O., Wilhelms, F., White, J.W.C., 2004. High-resolution record of Northern Hemisphere climate extending into the last interglacial period. Nature 431, 147–151. doi:10.1038/nature02805

Andrews, J.T., 2007. Holocene denudation of Iceland as determined from accumulation of sediments on the continental margin. Boreas 36, 240–252.

Andrews, J.T., 2005. Late Quaternary marine sediment studies of the Iceland shelf, Paleoceanography and land/ice sheet/ocean interactions, in: Caseldine, C., Russel, A., Hardardóttir, J., Knudsen, O. (Eds.), Iceland - Modern Processes and Past Environments. Elsevier, London, pp. 5–24.

Andrews, J.T., Cooper, T.A., Jennings, A.E., Stein, A.B., Erlenkeuser, H., 1998. Late Quaternary iceberg-rafted detritus events on the Denmark Strait–Southeast Greenland continental slope (~65°N): related to North Atlantic Heinrich events? Mar. Geol. 149, 211–228. doi:10.1016/S0025-3227(98)00029-2

Andrews, J.T., Geirsdóttir, A., Hardardóttir, J., Principato, S., Grönvold, K., Kristjansdóttir, G.B., Helgadóttir, G., Drexler, J., Sveinbjörnsdóttir, A., 2002a. Distribution, sediment magnetism and geochemistry of the Saksunarvatn (10 180 ± 60 cal. yr BP) tephra in marine, lake, and terrestrial sediments, northwest Iceland. J. Quat. Sci. 17, 731–745. doi:10.1002/jqs.727

Andrews, J.T., Hardardóttir, J., Geirsdóttir, Á., Helgadóttir, G., 2002b. Late Quaternary ice extent and glacial history from the Djúpáll trough, off Vestfirdir peninsula, north-west Iceland: a stacked 36 cal. Ky environmental record. Polar Res. 21, 211–226. doi:10.1111/j.1751-8369.2002.tb00074.x

Andrews, J.T., Hardardóttir, J., Helgadóttir, G., Jennings, A.E., Geirsdóttir, Á., Sveinbjörnsdóttir, Á.E., Schoolfield, S., Kristjánsdóttir, G.B., Smith, L.M., Thors, K., Syvitski, J.P.M., 2000. The N and W Iceland Shelf: insights into Last Glacial Maximum ice extent and deglaciation based on acoustic stratigraphy and basal radiocarbon AMS dates. Quat. Sci. Rev. 19, 619–631.

Andrews, J.T., Helgadóttir, G., 2003. Late Quaternary ice cap extent and deglaciation, Húnaflóaáll, northwest Iceland: evidence from marine cores. Arctic, Antarct. Alp. Res. 35, 218–232. doi:10.1657/1523-0430(2003)035[0218:LQICEA]2.0.CO;2

Andrews, J.T.T., 2008. The role of the Iceland Ice Sheet in the North Atlantic during the late Quaternary: a review and evidence from Denmark Strait. J. Quat. Sci. 23, 3–19. doi:10.1002/jqs

Ashwell, I.Y., 1975. Glacial and Late Glacial Processes in Western Iceland. Geogr. Ann. Ser. A, Phys. Geogr. 57, 225–245.

Auriac, A., Spaans, K.H., Sigmundsson, F., Hooper, A., Schmidt, P., Lund, B., 2013. Iceland rising: Solid Earth response to ice retreat inferred from satellite radar interferometry and visocelastic modeling. J. Geophys. Res. Solid Earth 118, 1331–1344. doi:10.1002/jgrb.50082

Ballantyne, C.K., 2010. Extent and deglacial chronology of the last British-Irish Ice Sheet: implications of exposure dating using cosmogenic isotopes. J. Quat. Sci. 25, 515–534. doi:10.1002/jqs.1310

Bamber, J.L., Griggs, J.A., Hurkmans, R.T.W.L., Dowdeswell, J.A., Gogineni, S.P., Howat, I., Mouginot,

1024 J., Paden, J., Palmer, S., Rignot, E., Steinhage, D., 2013. A new bed elevation dataset for
1025 Greenland. Cryosph. 7, 499–510. doi:10.5194/tc-7-499-2013

1026 Björnsson, H., Jónsson, T., Gylfadóttir, S.S., Ólason, E.O., 2007. Mapping the annual cycle of
1027 temperature in Iceland. Meteorol. Zeitschrift 16, 45–56.

1028 Blankenship, D.D., Bell, R.E., Hodge, S.M., Brozena, J.M., Behrendt, J.C., Finn, C.A., 1993. Active
1029 volcanism beneath the West Antarctic ice sheet and implications for ice-sheet stability. Nature
1030 361, 526–529.

1031 Blatter, H., 1995. Velocity and stress-fields in grounded glaciers - a simple algorithm for including
1032 deviatoric stress gradients. J. Glaciol. 41, 333–344. doi:10.3198/1995JoG41-138-333-344

1033 Boulton, G.S., Jarvis, J., Thors, K., 1988. Dispersal of glacially derived sediment over part of the
1034 continental shelf of south Iceland and the geometry of the resultant sediment bodies. Mar.
1035 Geol. 83, 193–223.

1036 Bourgeois, O., Dauteuil, O., Vliet-Lanoë, B. Van, 2000. Geothermal control on flow patterns in the
1037 Last Glacial Maximum ice sheet of Iceland. Earth Surf. Process. Landforms 25, 59–76.

1038 Brown, C.S., Meier, M.F., Post, A., 1982. Calving speed of Alaskan tidewater glaciers, with application
1039 to Columbia Glacier, US Geological Survey Professional Paper 1258-C.

1040 Brynjólfsson, S., Schomacker, A., Ingólfsson, Ó., Keiding, J.K., 2015. Cosmogenic 36Cl exposure ages
1041 reveal a 9.3 ka BP glacier advance and the Late Weichselian-Early Holocene glacial history of
1042 the Drangajökull region, northwest Iceland. Quat. Sci. Rev. 126, 140–157.
1043 doi:10.1016/j.quascirev.2015.09.001

1044 Caseldine, C., Geirsdóttir, Á., Langdon, P., 2003. Efstadalsvatn – a multi-proxy study of a Holocene
1045 lacustrine sequence from NW Iceland. J. Paleolimnol. 30, 55–73.
1046 doi:10.1023/A:1024781918181

1047 Chandler, D.M., Hubbard, A.L., Hubbard, B.P., Nienow, P.W., 2006. A Monte Carlo error analysis for
1048 basal sliding velocity calculations. J. Geophys. Res. Earth Surf. 111, F04005.
1049 doi:10.1029/2006JF000476

1050 Chauché, N., Hubbard, A., Gascard, J.-C., Box, J.E., Bates, R., Koppes, M., Sole, A., Christoffersen, P.,
1051 Patton, H., 2014. Ice–ocean interaction and calving front morphology at two west Greenland
1052 tidewater outlet glaciers. Cryosph. 8, 1457–1468. doi:10.5194/tc-8-1457-2014

1053 Clark, C.D., 1993. Mega-scale glacial lineations and cross-cutting ice-flow landforms. Earth Surf.
1054 Process. Landforms 18, 1–29.

1055 Clark, C.D., Hughes, A.L.C., Greenwood, S.L., Jordan, C., Sejrup, H.P., 2012. Pattern and timing of
1056 retreat of the last British-Irish Ice Sheet. Quat. Sci. Rev. 44, 112–146.
1057 doi:10.1016/j.quascirev.2010.07.019

1058 Clark, P.U., Dyke, A.S., Shakun, J.D., Carlson, A.E., Clark, J., Wohlfarth, B., Mitrovica, J.X., Hostetler,
1059 S.W., McCabe, a M., 2009. The Last Glacial Maximum. Science 325, 710–714.
1060 doi:10.1126/science.1172873

1061 Corr, H.F.J., Vaughan, D.G., 2008. A recent volcanic eruption beneath the West Antarctic ice sheet.
1062 Nat. Geosci. 1, 122–125. doi:10.1038/ngeo106

1063 Crochet, P., Jóhannesson, T., Jónsson, T., Sigur\dhsson, O., Björnsson, H., Pálsson, F., Barstad, I.,
1064 2007. Estimating the spatial distribution of precipitation in Iceland using a linear model of
1065 orographic precipitation. J. Hydrometeorol. 8, 1285–1306.

1066 Dansgaard, W., White, J.W.C., Johnsen, S.J., 1989. The abrupt termination of the Younger Dryas

1067 climate event. Nature 339, 532–534. doi:10.1038/339532a0

1068 Deschamps, P., Durand, N., Bard, E., Hamelin, B., Camoin, G., Thomas, A.L., Henderson, G.M., Okuno,
1069 J., Yokoyama, Y., 2012. Ice-sheet collapse and sea-level rise at the Bølling warming 14,600 years
1070 ago. Nature 483, 559–564. doi:10.1038/nature10902

1071 Dowdeswell, J.A., Evans, J., Ó Cofaigh, C., 2010. Submarine landforms and shallow acoustic
1072 stratigraphy of a 400 km-long fjord-shelf-slope transect, Kangerlussuaq margin, East Greenland.
1073 Quat. Sci. Rev. 29, 3359–3369. doi:10.1016/j.quascirev.2010.06.006

1074 Dyke, A., 2004. An outline of North American deglaciation with emphasis on central and northern
1075 Canada, in: Ehlers, J., Gibbard, P.L. (Eds.), Quaternary Glaciations - Extent and Chronology Part
1076 2: North America. Elsevier, pp. 371–406.

1077 Egloff, J., Johnson, G.L., 1979. Erosional and depositional structures of the southwest Iceland insular
1078 margin: thirteen geophysical profiles, in: Watkins, J.S., Montadert, L., Dickerson, P.W. (Eds.),
1079 Geological and Geophysical Investigations of Continental Margins, Geological and Geophysical
1080 Investigations of Continental Margins. American Association of Petroleum Geologists, Tulsa,
1081 Oklahoma, pp. 43–63.

1082 Einarsson, T., 1968. Jarðfræði, saga bergs og lands. Mál og Menning, Reykjavík.

1083 Eiríksson, J., Knudsen, K.L., Haflidason, H., Henriksen, P., 2000. Late-glacial and Holocene
1084 palaeoceanography of the North Icelandic shelf. J. Quat. Sci. 15, 23–42. doi:10.1002/(SICI)1099-
1085 1417(200001)15:1<23::AID-JQS476>3.0.CO;2-8

1086 Eiríksson, J., Símonarson, L.A., Knudsen, K.L., Kristensen, P., 1997. Fluctuations of the Weichselian ice
1087 sheet in SW Iceland: a glaciomarine sequence from Sudurnes, Seltjarnarnes. Quat. Sci. Rev. 16,
1088 221–240. doi:10.1016/S0277-3791(96)00052-2

1089 Engelhardt, H., 2004. Ice temperature and high geothermal flux at Siple Dome, West Antarctica,
1090 from borehole measurements. J. Glaciol. 50, 251–256. doi:10.3189/172756504781830105

1091 Fabel, D., Stroeven, A.P., Harbor, J., Kleman, J., Elmore, D., Fink, D., 2002. Landscape preservation
1092 under Fennoscandian ice sheets determined from in situ produced 10Be and 26Al. Earth Planet.
1093 Sci. Lett. 201, 397–406. doi:10.1016/S0012-821X(02)00714-8

1094 Fahnestock, M., Abdalati, W., Joughin, I., Brozena, J., Gogineni, P., 2001. High geothermal heat flow,
1095 basal melt, and the origin of rapid ice flow in central Greenland. Science 294, 2338–2342.

1096 Fisher, A.T., Mankoff, K.D., Tulaczyk, S.M., Tyler, S.W., Foley, N., 2015. High geothermal heat flux
1097 measured below the West Antarctic Ice Sheet. Sci. Adv. 1, e1500093–e1500093.
1098 doi:10.1126/sciadv.1500093

1099 Flóvenz, Ó.G., Sæmundsson, K., 1993. Heat flow and geothermal processes in Iceland.
1100 Tectonophysics 225, 123–138.

1101 Fretwell, P., Pritchard, H.D., Vaughan, D.G., Bamber, J.L., Barrand, N.E., Bell, R., Bianchi, C., Bingham,
1102 R.G., Blankenship, D.D., Casassa, G., Catania, G., Callens, D., Conway, H., Cook, A.J., Corr, H.F.J.,
1103 Damaske, D., Damm, V., Ferraccioli, F., Forsberg, R., Fujita, S., Gim, Y., Gogineni, P., Griggs, J.A.,
1104 Hindmarsh, R.C.A., Holmlund, P., Holt, J.W., Jacobel, R.W., Jenkins, A., Jokat, W., Jordan, T.,
1105 King, E.C., Kohler, J., Krabill, W., Riger-Kusk, M., Langley, K.A., Leitchenkov, G., Leuschen, C.,
1106 Luyendyk, B.P., Matsuoka, K., Mouginot, J., Nitsche, F.O., Nogi, Y., Nost, O.A., Popov, S. V.,
1107 Rignot, E., Rippin, D.M., Rivera, A., Roberts, J., Ross, N., Siegert, M.J., Smith, A.M., Steinhage,
1108 D., Studinger, M., Sun, B., Tinto, B.K., Welch, B.C., Wilson, D., Young, D.A., Xiangbin, C.,
1109 Zirizzotti, A., 2013. Bedmap2: improved ice bed, surface and thickness datasets for Antarctica.
1110 Cryosph. 7, 375–393. doi:10.5194/tc-7-375-2013

1111 Geirsdóttir, Á., 2011. Pliocene and Pleistocene Glaciations of Iceland: A Brief Overview of the Glacial
1112 History, in: Ehlers, Jürgen, Gibbard, P.L., Hughes, P.D. (Eds.), Quaternary Glaciations - Extent
1113 and Chronology. A Closer Look. Elsevier, pp. 199–260.

1114 Geirsdóttir, Á., Andrews, J.T., Ólafsdóttir, S., Helgadóttir, G., Hardardóttir, J., 2002. A 36 ka record of
1115 iceberg rafting and sedimentation from NW Iceland. Following the ice retreat from the shelf to
1116 land. Polar Res. 21, 291–298.

1117 Geirsdóttir, Á., Eiriksson, J., 1994. Sedimentary facies and environmental history of the Late-glacial
1118 glaciomarine Fossvogur sediments in Reykjavík, Iceland. Boreas 23, 164–176.
1119 doi:10.1111/j.1502-3885.1994.tb00597.x

1120 Geirsdóttir, Á., Hardardóttir, J., Eiríksson, J., 1997. The depositional history of the Younger Dryas-
1121 Preboreal Búði moraines in south-central Iceland. Arct. Alp. Res. 29, 13–23.

1122 Geirsdóttir, Á., Hardardóttir, J., Sveinbjörnsdóttir, Á.E., 2000. Glacial extent and catastrophic
1123 meltwater events during the deglaciation of Southern Iceland. Quat. Sci. Rev. 19, 1749–1761.

1124 Geirsdóttir, Á., Jennings, A.E., Lacasse, C., Hardadóttir, J., 1999. Record of jökullhlaup activities in
1125 Iceland during the late Younger Dryas and the Preboreal - evidence from land, near-shore, shelf
1126 and deep-sea sediments. Geol. Soc. Am. Abstr. with Programs 1, 314.

1127 Geirsdóttir, Á., Miller, G.H., Andrews, J.T., 2007. Glaciation, erosion, and landscape evolution of
1128 Iceland. J. Geodyn. 43, 170–186.

1129 Geirsdóttir, Á., Miller, G.H., Axford, Y., Sædís Ólafsdóttir, 2009. Holocene and latest Pleistocene
1130 climate and glacier fluctuations in Iceland. Quat. Sci. Rev. 28, 2107–2118.
1131 doi:10.1016/j.quascirev.2009.03.013

1132 Geyer, A., Bindeman, I., 2011. Glacial influence on caldera-forming eruptions. J. Volcanol. Geotherm.
1133 Res. 202, 127–142. doi:10.1016/j.jvolgeores.2011.02.001

1134 Glen, J., 1955. The creep of polycrystalline ice. Proc. R. Soc. London, Ser. A 228, 519–538.

1135 Golledge, N., Hubbard, A., Bradwell, T., 2010. Influence of seasonality on glacier mass balance, and
1136 implications for palaeoclimate reconstructions. Clim. Dyn. 35, 757–770. doi:10.1007/s00382-
1137 009-0616-6

1138 Golledge, N.R., Hubbard, A., Sugden, D.E., 2008. High-resolution numerical simulation of Younger
1139 Dryas glaciation in Scotland. Quat. Sci. Rev. 27, 888–904. doi:10.1016/j.quascirev.2008.01.019

1140 Greve, R., 2005. Relation of measured basal temperatures and the spatial distribution of the
1141 geothermal heat flux for the Greenland ice sheet. Ann. Glaciol. 42, 424–432.
1142 doi:10.3189/172756405781812510

1143 Greve, R., Hutter, K., 1995. Polythermal three-dimensional modelling of the Greenland ice sheet with
1144 varied geothermal heat flux. Ann. Glaciol. 21, 8–12.

1145 Grönvold, K., Oskarsson, N., Johnsen, S.J., Clausen, H.B., Hammer, C.U., Bond, G., Bard, E., 1995. Ash
1146 layers from Iceland in the Greenland GRIP ice core correlated with oceanic and land sediments.
1147 Earth Planet. Sci. Lett. 135, 149–155.

1148 Gudmundsson, M.T., Sigmundsson, F., Björnsson, H., 1997. Ice-volcano interaction of the 1996 Gjálp
1149 subglacial eruption, Vatnajökull, Iceland. Nature 389, 954–957. doi:10.1038/40122

1150 Håkansson, S., 1983. A reservoir age for the coastal waters of Iceland. Geol. Föreningen i Stock.
1151 Förhandlingar 105, 64–67. doi:10.1080/11035898309455300

1152 Hanna, E., Navarro, F.J., Pattyn, F., Domingues, C.M., Fettweis, X., Ivins, E.R., Nicholls, R.J., Ritz, C.,
1153 Smith, B., Tulaczyk, S., Whitehouse, P.L., Zwally, H.J., 2013. Ice-sheet mass balance and climate

change. Nature 498, 51–9. doi:10.1038/nature12238

Hindmarsh, R.C.A., 2004. A numerical comparison of approximations to the Stokes equations used in ice sheet and glacier modeling. J. Geophys. Res. Earth Surf. 109, F01012. doi:10.1029/2003JF000065

Hindmarsh, R.C.A., 1993. Modeling the dynamics of ice sheets. Prog. Phys. Geogr. 17, 391–412.

Hjartarson, Á., Ingólfsson, Ó., 1988. Preboreal glaciation of Southern Iceland. Jökull 38, 1–16.

Hjort, C., Ingólfsson, Ó., Norðdahl, H., 1985. Late Quaternary geology and glacial history of Hornstrandir, Northwest Iceland: a reconnaissance study. Jökull 38, 9–29.

Hoff, U., Rasmussen, T.L., Stein, R., Ezat, M.M., Fahl, K., 2016. Sea ice and millennial-scale climate variability in the Nordic seas 90 kyr ago to present. Nat. Commun. 7:12247. doi:10.1038/ncomms12247

Hoppe, G., 1968. Grimsey and the maximum extent of the last glaciation of Iceland. Geogr. Ann. Ser. A, Phys. Geogr. 50, 16–24.

Howat, I.M., Joughin, I., Scambos, T.A., 2007. Rapid changes in ice discharge from Greenland outlet glaciers. Science 315, 1559–61. doi:10.1126/science.1138478

Hubbard, A., 2006. The validation and sensitivity of a model of the Icelandic ice sheet. Quat. Sci. Rev. 25, 2297–2313. doi:10.1016/j.quascirev.2006.04.005

Hubbard, A., 2000. The verification and significance of three approaches to longitudinal stresses in high-resolution models of glacier flow. Geogr. Ann. Ser. A, Phys. Geogr. 82, 471–487. doi:10.1111/j.0435-3676.2000.00135.x

Hubbard, A., 1999. High-resolution modeling of the advance of the Younger Dryas ice sheet and its climate in Scotland. Quat. Res. 52, 27–43. doi:10.1006/qres.1999.2055

Hubbard, A., Blatter, H., Nienow, P., Mair, D., Hubbard, B., 1998. Comparison of a three-dimensional model for glacier flow with field data from Haut Glacier d'Arolla, Switzerland. J. Glaciol. 44, 368–378. doi:10.3198/1998JoG44-147-368-378

Hubbard, A., Bradwell, T., Golledge, N., Hall, A., Patton, H., Sugden, D., Cooper, R., Stoker, M., 2009. Dynamic cycles, ice streams and their impact on the extent, chronology and deglaciation of the British–Irish ice sheet. Quat. Sci. Rev. 28, 758–776. doi:10.1016/j.quascirev.2008.12.026

Hubbard, A., Hein, A.S., Kaplan Michael, R., Hulton, N.R.J., Glasser, N.F., 2005. A modelling reconstruction of the last glacial maximum ice sheet and its deglaciation in the vicinity of the Northern Patagonian Icefield, South America. Geogr. Ann. Ser. A, Phys. Geogr. 87, 375–391. doi:10.1111/j.0435-3676.2005.00264.x

Hubbard, A., Sugden, D., Dugmore, A., Norddahl, H., Pétursson, H.G., 2006. A modelling insight into the Icelandic Last Glacial Maximum ice sheet. Quat. Sci. Rev. 25, 2283–2296. doi:10.1016/j.quascirev.2006.04.001

Hubbard, B.P., Hubbard, A., Mader, H.M., Tison, J.-L., Grust, K., Nienow, P.W., 2003. Spatial variability in the water content and rheology of temperate glaciers: Glacier de Tsanfleuron, Switzerland. Ann. Glaciol. 37, 1–6. doi:10.3189/172756403781815474

Hughes, A.L.C., Gyllencreutz, R., Lohne, Ø.S., Mangerud, J., Svendsen, J.I., 2016. The last Eurasian ice sheets – a chronological database and time-slice reconstruction, DATED-1. Boreas 45, 1–45. doi:10.1111/bor.12142

Ingólfsson, Ó., 1991. A review of the Late Weischelian and early Holocene glacial and environmental history of Iceland, in: Caseldine, C., Maizels, J.K. (Eds.), Environmental Change in Iceland: Past

and Present. Kluwer Academic Publishers, Netherlands, pp. 13–29.

Ingólfsson, Ó., Björck, S., Haflidason, H., Rundgren, M., 1997. Glacial and climatic events in iceland reflecting regional north atlantic climatic shifts during the Pleistocene-Holocene transition. Quat. Sci. Rev. 16, 1135–1144. doi:10.1016/S0277-3791(97)00007-3

Ingólfsson, Ó., Norðdahl, H., 2001. High relative sea level during the Bølling Interstadial in western Iceland: a reflection of ice-sheet collapse and extremely rapid glacial unloading. Arctic, Antarct. Alp. Res. 33, 231–243.

Ingólfsson, Ó., Norðdahl, H., 1994. A review of the environmental history of Iceland, 13,000-9000 yr BP. J. Quat. Sci. 9, 147–150.

Ingólfsson, Ó., Norðdahl, H., Haflidason, H., 1995. Rapid isostatic rebound in southwestern Iceland at the end of the last glaciation. Boreas 24, 245–259. doi:10.1111/j.1502-3885.1995.tb00777.x

Ingólfsson, Ó., Norðdahl, H., Schomacker, A., 2010. Deglaciation and Holocene Glacial History of Iceland, in: The Mýrdalsjökull Ice Cap, Iceland. Glacial Processes, Sediments and Landforms on an Active Volcano, Developments in Quaternary Sciences. Elsevier, pp. 51–68. doi:10.1016/S1571-0866(09)01304-9

Jakobsson, S.P., Jónsson, J., Shido, F., 1978. Petrology of the western Reykjanes Peninsula, Iceland. J. Petrol. 19, 669–705.

Jennings, A., Syvitski, J.P.M., Gerson, L., 2000. Chronology and paleoenvironments during the late Weichselian deglaciation of the southwest Iceland shelf. Boreas 29, 163–183.

Jull, M., McKenzie, D., 1996. The effect of deglaciation on mantle melting beneath Iceland. J. Geophys. Res. Solid Earth 101, 21815–21828.

Keith, D.B., Jones, E.W., 1935. Grímsey, North Iceland. Geogr. Journal1 86, 143–152.

King, E.C., Hindmarsh, R.C.A., Stokes, C.R., 2009. Formation of mega-scale glacial lineations observed beneath a West Antarctic ice stream. Nat. Geosci. 2, 585–588.

Koenigk, T., Mikolajewicz, U., Jungclaus, J.H., Kroll, A., 2009. Sea ice in the Barents Sea: seasonal to interannual variability and climate feedbacks in a global coupled model. Clim. Dyn. 32, 1119–1138. doi:10.1007/s00382-008-0450-2

Kukkonen, I.T., 1989. Terrestrial heat flow and radiogenic heat production in Finland, the central Baltic Shield. Tectonophysics 164, 219–230. doi:10.1016/0040-1951(89)90015-2

Lambeck, K., Rouby, H., Purcell, A., Sun, Y., Sambridge, M., 2014. Sea level and global ice volumes from the Last Glacial Maximum to the Holocene. Proc. Natl. Acad. Sci. U. S. A. 111, 15296–303. doi:10.1073/pnas.1411762111

Larsen, D.J., Miller, G.H., Geirsdóttir, Á., Ólafsdóttir, S., 2012. Non-linear Holocene climate evolution in the North Atlantic: a high-resolution, multi-proxy record of glacier activity and environmental change from Hvítárvatn, central Iceland. Quat. Sci. Rev. 39, 14–25. doi:10.1016/j.quascirev.2012.02.006

Laumann, T., Reeh, N., 1993. Sensitivity to climate-change of the mass-balance of glaciers in southern Norway. J. Glaciol. 39, 656–665. doi:10.3198/1993JoG39-133-656-665

Licciardi, J.M., Kurz, M.D., Curtice, J.M., 2007. Glacial and volcanic history of Icelandic table mountains from cosmogenic 3He exposure ages. Quat. Sci. Rev. 26, 1529–1546. doi:10.1016/j.quascirev.2007.02.016

Lubimova, E.., Karus, E.., Firsov, F.., Starikova, G.., Vlasov, V.., Lyusova, L.., Koperbakh, E.., 1972. Terrestrial heat flow on Pre-Cambrian shields in the USSR. Geothermics 1, 81–89.

1240 doi:10.1016/0375-6505(72)90017-X

1241 MacAyeal, D.R., 1993. Binge/purge oscillations of the Laurentide Ice Sheet as a cause of the North
1242 Atlantic's Heinrich Events. Paleoceanography 8, 775–784.

1243 Maclennan, J., Jull, M., McKenzie, D., Slater, L., Grönvold, K., 2002. The link between volcanism and
1244 deglaciation in Iceland. Geochemistry, Geophys. Geosystems 3, 1–25.
1245 doi:10.1029/2001GC000282

1246 Mangerud, J., Gulliksen, S., Larsen, E., 2010. 14C-dated fluctuations of the western flank of the
1247 Scandinavian Ice Sheet 45-25 kyr BP compared with Bølling-Younger Dryas fluctuations and
1248 Dansgaard-Oeschger events in Greenland. Boreas 39, 328–342. doi:10.1111/j.1502-
1249 3885.2009.00127.x

1250 Mangerud, J., Gulliksen, S., Larsen, E., Longva, O., Miller, G.H., Sejrup, H.-P., Sønstegaard, E., 1981. A
1251 Middle Weichselain ice-free period in Western Norway: the Ålesund Interstadial. Boreas 10,
1252 447–462. doi:10.1111/j.1502-3885.1981.tb00508.x

1253 Marshall, S.J., Björnsson, H., Flowers, G.E., Clarke, G.K.C., 2005. Simulation of Vatnajökull ice cap
1254 dynamics. J. Geophys. Res. Earth Surf. 110, F03009. doi:10.1029/2004JF000262

1255 Maule, C.F., Purucker, M.E., Olsen, N., Mosegaard, K., 2005. Heat flux anomalies in Antarctica
1256 revealed by satellite magnetic data. Science 309, 464–467. doi:10.1126/science.1106888

1257 Näslund, J.-O., Jansson, P., Fastook, J.L., Johnson, J., Andersson, L., 2005. Detailed spatially
1258 distributed geothermal heat-flow data for modeling of basal temperatures and meltwater
1259 production beneath the Fennoscandian ice sheet. Ann. Glaciol. 40, 95–101.
1260 doi:10.3189/172756405781813582

1261 Nick, F.M., Luckman, A., Vieli, A., van der Veen, C.J., van As, D., van de Wal, R.S.W., Pattyn, F.,
1262 Hubbard, A.L., Floricioiu, D., 2012. The response of Petermann Glacier, Greenland, to large
1263 calving events, and its future stability in the context of atmospheric and oceanic warming. J.
1264 Glaciol. 58, 229–239. doi:10.3189/2012JoG11J242

1265 Nielsen, T., Rasmussen, T.L., Ceramicola, S., Kuijpers, A., 2007. Quaternary sedimentation, margin
1266 architecture and ocean circulation variability around the Faroe Islands, North Atlantic. Quat.
1267 Sci. Rev. 26, 1016–1036. doi:10.1016/j.quascirev.2006.12.005

1268 Norðdahl, H., 1991. A review of the glaciation maximum concept and the deglacation of Eyjafjördur,
1269 North Iceland, in: Maizels, J.K., Caseldine, C. (Eds.), Environmental Change in Iceland: Past and
1270 Present. Kluwer Academic Publishers, Netherlands, pp. 31–47.

1271 Norðdahl, H., 1983. Late Quaternary stratigraphy of Fnjóskadalur, central North Iceland: a study of
1272 sediments, ice-lake strandlines, glacial isostasy and ice-free areas. Lundqua Thesis 12, Lundqua
1273 thesis. Lund University.

1274 Norðdahl, H., Einarsson, T., 2001. Concurrent changes of relative sea-level and glacier extent at the
1275 Weichselian-Holocene boundary in Berufjörður, Eastern Iceland. Quat. Sci. Rev. 20, 1607–1622.

1276 Norðdahl, H., Haflidason, H., 1992. The Skógar Tephra, a Younger Dryas marker in North Iceland.
1277 Boreas 21, 23–41.

1278 Norðdahl, H., Hjort, C., 1995. Lateglacial raised beaches and glacier recession in the Thistilfjörður-
1279 Bakkaflói area, northeast Iceland. Jökull 43, 32–44.

1280 Norðdahl, H., Ingólfsson, Ó., 2015. Collapse of the Icelandic ice sheet controlled by sea-level rise?
1281 Arktos 1, 1–13. doi:10.1007/s41063-015-0020-x

1282 Norðdahl, H., Ingólfsson, Ó., Pétursson, H.G., Hallsdóttir, M., 2008. Late Weichselian and Holocene

1283 environmental history of Iceland. Jökull 58, 343–364.

1284 Norðdahl, H., Pétursson, G.P., 2005. Relative sea level changes in Iceland: new aspect of the
1285 Weichselian deglaciation of Iceland, in: Caseldine, C., Russel, A., Hardardóttir, J., Knudsen, O.
1286 (Eds.), Iceland - Modern Processes and Past Environments. Elsevier, Amsterdam, pp. 25–78.

1287 Ó Cofaigh, C., 1996. Tunnel valley genesis. Prog. Phys. Geogr. 20, 1–19.
1288 doi:10.1177/030913339602000101

1289 Ó Cofaigh, C., Pudsey, C.J., Dowdeswell, J.A., Morris, P., 2002. Evolution of subglacial bedforms along
1290 a paleo-ice stream, Antarctic Peninsula continental shelf. Geophys. Res. Lett. 29, 1199.

1291 Óladóttir, B.A., Larsen, G., Sigmarsson, O., 2011. Holocene volcanic activity at Grímsvötn,
1292 Bárdarbunga and Kverkfjöll subglacial centres beneath Vatnajökull, Iceland. Bull. Volcanol. 73,
1293 1187–1208. doi:10.1007/s00445-011-0461-4

1294 Ólafsdóttir, T., 1975. Jökulgardur á sjávarbotniit af Breidafirdi (English summary: A moraine ridge on
1295 the Iceland shelf, west of Breidafjördur). Náttúrufrædingurinn 45, 247–271.

1296 Ottesen, D., Dowdeswell, J.A., Rise, L., Rokoengen, K., Henriksen, S., 2002. Large-scale morphological
1297 evidence for past ice-stream flow on the mid-Norwegian continental margin. Geol. Soc.
1298 London, Spec. Publ. 203, 245–258.

1299 Papa, B.D., Mysak, L.A., Wang, Z., 2005. Intermittent ice sheet discharge events in northeastern
1300 North America during the last glacial period. Clim. Dyn. 26, 201–216. doi:10.1007/s00382-005-
1301 0078-4

1302 Patton, H., Andreassen, K., Bjarnadóttir, L.R., Dowdeswell, J.A., Winsborrow, M.C.M., Noormets, R.,
1303 Polyak, L., Auriac, A., Hubbard, A., 2015. Geophysical constraints on the dynamics and retreat
1304 of the Barents Sea Ice Sheet as a palaeo-benchmark for models of marine ice-sheet
1305 deglaciation. Rev. Geophys. 53, 1051–1098. doi:10.1002/2015RG000495

1306 Patton, H., Hubbard, A., Andreassen, K., Winsborrow, M., Stroeven, A.P., 2016. The build-up,
1307 configuration, and dynamical sensitivity of the Eurasian ice-sheet complex to Late Weichselian
1308 climatic and oceanic forcing. Quat. Sci. Rev. 153, 97–121. doi:10.1016/j.quascirev.2016.10.009

1309 Patton, H., Hubbard, A., Glasser, N.F., Bradwell, T., Golledge, N.R., 2013. The last Welsh Ice Cap: Part
1310 1 - Modelling its evolution, sensitivity and associated climate. Boreas 42, 471–490.
1311 doi:10.1111/j.1502-3885.2012.00300.x

1312 Pattyn, F., Perichon, L., Aschwanden, A., Breuer, B., de Smedt, B., Gagliardini, O., Gudmundsson,
1313 G.H., Hindmarsh, R.C.A., Hubbard, A., Johnson, J. V, Kleiner, T., Konovalov, Y., Martin, C., Payne,
1314 A.J., Pollard, D., Price, S., Rückamp, M., Saito, F., Souček, O., Sugiyama, S., Zwinger, T., 2008.
1315 Benchmark experiments for higher-order and full-Stokes ice sheet models (ISMIP–HOM).
1316 Cryosph. 2, 95–108. doi:10.5194/tc-2-95-2008

1317 Peltier, W.R., Fairbanks, R.G., 2006. Global glacial ice volume and Last Glacial Maximum duration
1318 from an extended Barbados sea level record. Quat. Sci. Rev. 25, 3322–3337.
1319 doi:10.1016/j.quascirev.2006.04.010

1320 Pétursson, H.G., 1991. The Weichselian glacial history of West Melrakkaslétta, Northeastern Iceland,
1321 in: Maizels, J.M., Caseldine, C. (Eds.), Environmental Change in Iceland: Past and Present.
1322 Kluwer Academic Publishers, Dordrecht, pp. 49–65.

1323 Pétursson, H.G., Norðdahl, H., Ingólfsson, Ó., 2015. Late Weichselian history of relative sea level
1324 changes in Iceland during a collapse and subsequent retreat of marine based ice sheet. Cuad.
1325 Investig. Geográfica 41, 261. doi:10.18172/cig.2741

1326 Pollard, D., DeConto, R.M., 2007. A coupled ice-sheet/ice-shelf/sediment model applied to a marine-

margin flowline: forced and unforced variations., in: Hambrey, M.J., Christoffersen, P., Glasser, N.F., Hubbard, B. (Eds.), Glacial Sedimentary Processes and Products. Blackwell Publishing Ltd, Oxford.

Principato, S.M., Geirsdóttir, Á., Jóhannsdóttir, G.E., Andrews, J.T., 2006. Late Quaternary glacial and deglacial history of eastern Vestfirdir, Iceland using cosmogenic isotope (36Cl) exposure ages and marine cores. J. Quat. Sci. 21, 271–285. doi:10.1002/jqs.978

Principato, S.M., Jennings, A.E., Kristjansdottir, G.B., Andrews, J.T., 2005. Glacial-Marine or Subglacial Origin of Diamicton Units from the Southwest and North Iceland Shelf: Implications for the Glacial History of Iceland. J. Sediment. Res. 75, 968–983. doi:10.2110/jsr.2005.073

Principato, S.M., Johnson, J.S., 2009. Using a GIS to Quantify Patterns of Glacial Erosion on Northwest Iceland: Implications for Independent Ice Sheets. Arctic, Antarct. Alp. Res. 41, 128–137. doi:10.1657/1523-0430-41.1.128

Principato, S.M., Moyer, A.N., Hampsch, A.G., Ipsen, H.A., 2016. Using GIS and streamlined landforms to interpret palaeo-ice flow in northern Iceland. Boreas n/a-n/a. doi:10.1111/bor.12164

Quillmann, U., Andrews, J.T., Jennings, A.E., 2009. Radiocarbon Date List XI : Radiocardon dates from Marine Sediment Cores of the Iceland, Greenland and the Northeast Canada Arctic Shelves and Nares Strait. Instaar/OP Occasional.

Rasmussen, S.O., Bigler, M., Blockley, S.P., Blunier, T., Buchardt, S.L., Clausen, H.B., Cvijanovic, I., Dahl-Jensen, D., Johnsen, S.J., Fischer, H., Gkinis, V., Guillevic, M., Hoek, W.Z., Lowe, J.J., Pedro, J.B., Popp, T., Seierstad, I.K., Steffensen, J.P., Svensson, A.M., Vallelonga, P., Vinther, B.M., Walker, M.J.C., Wheatley, J.J., Winstrup, M., 2014. A stratigraphic framework for abrupt climatic changes during the Last Glacial period based on three synchronized Greenland ice-core records: Refining and extending the INTIMATE event stratigraphy. Quat. Sci. Rev. 106, 14–28. doi:10.1016/j.quascirev.2014.09.007

Reimer, P., Bard, E., Bayliss, A., Beck, J.W., Blackwell, P.G., Ramsey, C.B., Buck, C.E., Cheng, H., Edwards, R.L., Friedrich, M., Grootes, P.M., Guilderson, T.P., Haflidason, H., Hajdas, I., Hatté, C., Heaton, T.J., Hoffmann, D.L., Hogg, A.G., Hughen, K.A., Kaiser, K.F., Kromer, B., Manning, S.W., Niu, M., Reimer, R.W., Richards, D.A., Scott, E.M., Southon, J.R., Staff, R.A., Turney, C.S.M., Plicht, J. van der, 2013. IntCal13 and Marine13 Radiocarbon Age Calibration Curves 0–50,000 Years cal BP. Radiocarbon 55, 1869–1887. doi:10.2458/azu_js_rc.55.16947

Rignot, E., Kanagaratnam, P., 2006. Changes in the velocity structure of the Greenland ice sheet. Science 311, 986–990.

Rignot, E., Koppes, M., Velicogna, I., 2010. Rapid submarine melting of the calving faces of West Greenland glaciers. Nat. Geosci. 3, 187–191. doi:10.1038/ngeo765

Roberts, D.H., Long, A.J., Schnabel, C., Freeman, S., Simpson, M.J.R., 2008. The deglacial history of southeast sector of the Greenland Ice Sheet during the Last Glacial Maximum. Quat. Sci. Rev. 27, 1505–1516. doi:10.1016/j.quascirev.2008.04.008

Rogozhina, I., Hagedoorn, J.M., Martinec, Z., Fleming, K., Soucek, O., Greve, R., Thomas, M., 2012. Effects of uncertainties in the geothermal heat flux distribution on the Greenland Ice Sheet: An assessment of existing heat flow models. J. Geophys. Res. 117, F02025.

Rogozhina, I., Petrunin, A.G., Vaughan, A.P.M., Steinberger, B., Johnson, J. V., Kaban, M.K., Calov, R., Rickers, F., Thomas, M., Koulakov, I., 2016. Melting at the base of the Greenland ice sheet explained by Iceland hotspot history. Nat. Geosci. 9, 366–369. doi:10.1038/ngeo2689

Rolandone, F., Mareschal, J.-C., Jaupart, C., 2003. Temperatures at the base of the Laurentide Ice

1372 Sheet inferred from borehole temperature data. Geophys. Res. Lett. 30.
1373 doi:10.1029/2003GL018046

1374 Rott, H., Rack, W., Skvarca, P., De Angelis, H., 2002. Northern Larsen Ice Shelf, Antarctica: further
1375 retreat after collapse. Ann. Glaciol. 34, 277–282.

1376 Rundgren, M., Ingólfsson, Ó., 1999. Plant survival in Iceland during periods of glaciation? J. Biogeogr.
1377 26, 387–396. doi:10.1046/j.1365-2699.1999.00296.x

1378 Rundgren, M., Ingólfsson, Ó., Björck, S., Jiang, H., Haflidason, H., 1997. Dynamic sea-level change
1379 during the last deglaciation of northern Iceland. Boreas 26, 201–215. doi:10.1111/j.1502-
1380 3885.1997.tb00852.x

1381 Shepherd, A., Ivins, E.R., A, G., Barletta, V.R., Bentley, M.J., Bettadpur, S., Briggs, K.H., Bromwich,
1382 D.H., Forsberg, R., Galin, N., Horwath, M., Jacobs, S., Joughin, I., King, M.A., Lenaerts, J.T.M., Li,
1383 J., Ligtenberg, S.R.M., Luckman, A., Luthcke, S.B., McMillan, M., Meister, R., Milne, G.,
1384 Mouginot, J., Muir, A., Nicolas, J.P., Paden, J., Payne, A.J., Pritchard, H., Rignot, E., Rott, H.,
1385 Sørensen, L.S., Scambos, T.A., Scheuchl, B., Schrama, E.J.O., Smith, B., Sundal, A. V, van
1386 Angelen, J.H., van de Berg, W.J., van den Broeke, M.R., Vaughan, D.G., Velicogna, I., Wahr, J.,
1387 Whitehouse, P.L., Wingham, D.J., Yi, D., Young, D., Zwally, H.J., 2012. A reconciled estimate of
1388 ice-sheet mass balance. Science 338, 1183–9. doi:10.1126/science.1228102

1389 Siegert, M.J., Dowdeswell, J.A., 1996. Topographic control on the dynamics of the Svalbard-Barents
1390 Sea ice sheet. Glob. Planet. Change 12, 27–39. doi:10.1016/0921-8181(95)00010-0

1391 Sigmundsson, F., 1991. Post-glacial rebound and asthenosphere viscosity in Iceland. Geophys. Res.
1392 Lett. 18, 1131–1134. doi:10.1029/91GL01342

1393 Sigvaldason, G.E., Annertz, K., Nilsson, M., 1992. Effect of glacier loading/deloading on volcanism:
1394 postglacial volcanic production rate of the Dyngjufjöll area, central Iceland. Bull. Volcanol. 54,
1395 385–392.

1396 Sinton, J., Grönvold, K., Saemundsson, K., 2005. Postglacial eruptive history of the Western Volcanic
1397 Zone, Iceland. Geochemistry Geophys. Geosystems 6, Q12009.

1398 Slater, L., Jull, M., McKenzie, D., Gronvöld, K., 1998. Deglaciation effects on mantle melting under
1399 Iceland: results from the northern volcanic zone. Earth Planet. Sci. … 164, 151–164.

1400 Smellie, J.L., 2000. Subglacial eruptions, in: Sigurdsson, H. (Ed.), Encyclopedia of Volcanoes.
1401 Academic Press, San Diego, pp. 403–418.

1402 Spagnolo, M., Clark, C.D., 2009. A geomorphological overview of glacial landforms on the Icelandic
1403 continental shelf. J. Maps 5, 37–52. doi:10.4113/jom.2009.1049

1404 Stokes, C.R., Clark, C.D., 2002. Are long subglacial bedforms indicative of fast ice flow? Boreas 31,
1405 239–249. doi:10.1111/j.1502-3885.2002.tb01070.x

1406 Stokes, C.R., Clark, C.D., 2001. Palaeo-ice streams. Quat. Sci. Rev. 20, 1437–1457.

1407 Stokes, C.R., Margold, M., Clark, C.D., Tarasov, L., 2016. Ice stream activity scaled to ice sheet volume
1408 during Laurentide Ice Sheet deglaciation. Nature 530, 322–326. doi:10.1038/nature16947

1409 Stötter, J., Wastl, M., Caseldine, C., Häberle, T., 1999. Holocene palaeoclimatic reconstruction in
1410 northern Iceland: approaches and results. Quat. Sci. Rev. 18, 457–474. doi:10.1016/S0277-
1411 3791(98)00029-8

1412 Stuiver, M., Reimer, P., 1993. Extended 14C Data Base and Revised Calib 3.0 14C Age Calibration
1413 Program. Radiocarbon 35, 215–230.

1414 Syvitski, J.P., Burrell, D.C., Skei, J.M., 1987. Fjords: Processes and Products. Springer Verlag, New

1415 York.

1416 Syvitski, J.P., Jennings, A.E., Andrews, J.T., 1999. High-resolution seismic evidence for multiple
1417 glaciation across the southwest Iceland Shelf. Arctic, Antarct. Alp. Res. 31, 50–57.

1418 Tarasov, L., Peltier, W.R., 2003. Greenland glacial history, borehole constraints, and Eemian extent. J.
1419 Geophys. Res. 108, 2143. doi:10.1029/2001JB001731

1420 Thomas, E.R., Mulvaney, R., Wolff, E.W., 2008. A change in seasonality in Greenland during a
1421 Dansgaard–Oeschger warming. Ann. Glaciol. 48, 19–24. doi:10.3189/172756408784700590

1422 Thordarson, T., Larsen, G., 2007. Volcanism in Iceland in historical time: Volcano types, eruption
1423 styles and eruptive history. J. Geodyn. 43, 118–152. doi:10.1016/j.jog.2006.09.005

1424 Van Vliet-Lanoë, B., Gudmundsson, Å., Guillou, H., Duncan, R. a., Genty, D., Ghaleb, B., Gouy, S.,
1425 Récourt, P., Scaillet, S., 2007. Limited glaciation and very early deglaciation in central Iceland.
1426 Comptes Rendus Geosci. 339, 1–12. doi:10.1016/j.crte.2006.12.001

1427 Vasskog, K., Langebroek, P.M., Andrews, J.T., Nilsen, J.E.Ø., Nesje, A., 2015. The Greenland Ice Sheet
1428 during the last glacial cycle: Current ice loss and contribution to sea-level rise from a
1429 palaeoclimatic perspective. Earth-Science Rev. 150, 45–67. doi:10.1016/j.earscirev.2015.07.006

1430 Vilmundardóttir, E., Larsen, G., 1986. Productivity pattern of the Veidivötn fissure swarm, Southern
1431 Iceland, in post-glacial times. Preliminary results. 17e Nord. Geol. Helsinki.

1432 Vogel, S.W., Tulaczyk, S., 2006. Ice-dynamical constraints on the existence and impact of subglacial
1433 volcanism on West Antarctic ice sheet stability. Geophys. Res. Lett. 33, L23502.
1434 doi:10.1029/2006GL027345

1435 Walker, G.P.L., 1965. Some aspects of Quaternary volcanism in Iceland. Trans. Leicester Lit. Philos.
1436 Soc. 59, 25–40.

1437 Weertman, J., 1964. The theory of glacier sliding. J. Glaciol. 5, 287–303.

1438 Winberry, J.P., Anandakrishnan, S., 2004. Crustal structure of the West Antarctic rift system and
1439 Marie Byrd Land hotspot. Geology 32, 977–980.

1440 Winsborrow, M.C.M., Andreassen, K., Corner, G.D., Laberg, J.S., 2010. Deglaciation of a marine-
1441 based ice sheet: Late Weichselian palaeo-ice dynamics and retreat in the southern Barents Sea
1442 reconstructed from onshore and offshore glacial geomorphology. Quat. Sci. Rev. 29, 424–442.
1443 doi:10.1016/j.quascirev.2009.10.001

1444

Core/Lab ID	Source	Lat N	Long W	Uncorrected age (^{14}C yr BP)	Median probability age (cal. ka BP)		Notes
Jökuldjúp							
AA-12896	Syvitski et al. [1999]; Jennings et al. [2000]	64 17.06	24 12.42	13,105 ± 85	15,068	14,652 – 15,368	*N. labradorica* found in glacial marine unit with dropstones. Within 1 m of the underlying ice contact deposit. Sampled from the core cutter.
MD99-2256	Principato et al. [2005]	64 18.19	24 12.4	12,990 ± 80	14,850	14,337 – 15,174	Mollusc at base of glacimarine sediments
Latra Bank							
96-1227GGC	Syvitski et al. [1999]	65 47.0	26 19.5	36,050 ± 560	40,215	38,970 – 41,369	*Cibicides lobatulus* from possible exposed older (pre LGM) sediments due to glacial erosion
96-1220GGC	Andrews et al. [2000]	65 0.0	27 30.0	18,090 ± 80	21,364	21,045 – 21,660	*N. pachyderma*
JM96-1221GGC		65 7.9	27 32.2	18,240 ± 80	21,579	21,301 – 21,849	
Djúpáll							
JM96-1234GGC	Andrews et al. [2000]	66 35.15	23 58.8	15,720 ± 70	18,564	18,373 – 18,735	Mixed benthics from the base of core.
B997-338PC	Andrews et al. [2002]	66 35.3	23 58.6	19,280 ± 420	22,761	21,809 – 23,759	Sample located within rhythmic laminations above diamict. Material unreported.
				34,600 ± 640	38,599	36,771 – 40,056	Unreported foraminifera within diamict underlying laminated marine deposits
Northern troughs							
97-317PC	Andrews et al. [2000]	66 35.27	18 51.9	12,270 ± 100	13,702	13,454 – 13,947	*N. labradoricum* and *C. teretis*
B997-322PC		66 56.29	19 6.5	42,600 ± 3,050	45,590	41,333 – *	Mixed benthic and planktic forams c. 1 m within massive matrix supported diamicton.
B997-323PC1	Andrews & Helgadóttir [2003]	66 50.78	20 13.64	25,330 ± 640	29,018	27,776 – 30,457	Mixed benthic and planktic forams, c. 2 m within massive matrix supported diamicton.
				13,440 ± 190	15,569	15,021 – 16,166	Mixed benthic and planktic forams, at the base of glacimarine muds above massive matrix supported diamicton (till).
B997-326PC1	Principato et al. [2005]	66 36.35	20 54.82	13,835 ± 215	16,133	15,457 – 16,810	Mixed benthic and planktic foraminifera within fine-grained sediments (marine).
	Andrews & Helgadóttir [2003]			23,570 ± 340	27,385	26,615 – 27,892	Mixed benthic foraminifera at the interface between massive matrix supported diamicton and fine-grained sediments (marine).
HM107-04	Eiríksson et al. [2000]	67 13.63	19 3.0	12,040 ± 80	13,464	13,292 – 13,675	Foraminifera, total benthic fauna within marine sediments
HM107-05		66 54.32	17 54.31	14,100 ± 140	16,506	16,102 – 16,969	Foraminifera, *Neogloboquadrina pachyderma* sinistral
Búdi moraines							

AAR-1241	Geirsdóttir et al. [1997]	Búdafoss	10,290 ± 140	11,340	10,943 – 11,878	*Balanus balanus* within uppermost glaciomarine unit
Lu-2403	Hjartarson and Ingólfsson [1988]	Búdafoss	10,220 ± 90	11,197	10,938 – 11,563	*Balanus balanus* on the surface of diamictite
Reykjanesskagi						
U-2898	Norðdahl [1991]	Varmá, Helgafelssmelar	10,780 ± 110	12,197	11,796 – 12,566	*Balanus balanus* collected in the lowermost part of a gravel pit in a raised terrace
AAR-2803	Jóhannesson et al. [1997]; Norðdahl & Pétursson [2005]	Sandgerði	24,510 ± 200	28,130	27,751 – 28,567	*Hyatella arctica* shell fragments from basal till atop striated (215°) bedrock
AAR-2573 - AAR-2577; Beta-82638		Njarðvíkurheiði	21,890 ± 105	25,777	25,561 – 25,976	Weighted mean age from 6 marine shell samples from stratified silty fine sand resting on glacially striated (9°) bedrock
AAR-1900	Eiríksson et al. [1997]	Sudernes	28,100 ± 410	31,571	30,954 – 32,640	*Mya truncata samples* within marine, bioturbated diamictite above subglacial tillite and glacially striated (340°) lava flow.
AAR-1901			28,750 ± 480	32,288	31,289 – 33,441	
Western Iceland						
S-291	Ashwell [1975]	Grjóteyri	12,800 ± 200	14,504	13,884 – 15,170	Shells within marine drift 15-21 m a.s.l.
AAR-3734	Magnusdóttir & Norðdahl	Stora-Fellsöxl	12,940 ± 80	14,736	14,268 – 15,111	Whalebone 80 m a.s.l., constraining a marine limit of 105 m a.s.l.
Ua-21222	Ingólfsson & Norðdahl [2001]	Stóri-Sandhóll	12,975 ± 105	14,792	14,252 – 15,185	Mollusc 135 m a.s.l., constraining a marine limit of 150 m a.s.l.
Lu-3118	Ingólfsson et al. [1995]	Helgafellsmelar	10,580 ± 90	11,793	11,327 – 12,158	*Balanus balanus* shells in sandy layers within a glacimarine diamicton unit, above subglacial till.
Eastern Iceland						
T-4468	Pétursson 1986	Hvalvik	13,020 ± 90	14,898	14,363 – 15,236	Constraining a marine limit 50-60 m a.s.l.

** Radiocarbon age exceeds the upper calibration curve range.*

Parameter		Value	Units
g	Gravity	9.81	m s^{-2}
ρ	Density of ice	910	kg m^{-3}
ρ_w	Density of sea water	1028	kg m^{-3}
N	Glen flow-law exponent	3	
A_{weert}	Weertman sliding parameter	7.5×10^{-14}	
m	Sliding-law exponent	1 – 3	
SF	Sliding factor	5	
A_s	Sliding-law coefficient	1.8×10^{-5}	m kPa^{-3} a^{-1}
A_0	Deformation enhancement	2.5	
A_c	Calving parameter	24.4	a^{-1}
PDD_{ice}	PDD coefficient for ice	0.008	m °C m^{-1} d^{-1}
PDD_{snow}	PDD coefficient for snow|	0.003	m °C m^{-1} d^{-1}
T	Temperature	-	K
T^*	(pressure melt corrected)	$T - 8.7 \times 10^{-4} (S - z)$	K
$T_{snow\text{-}rain}$	Snow-rain threshold	1.0	°C
R	Gas constant	8.314	J mol^{-1} K^{-1}
k_i	Thermal conductivity	2115.3 + 7.93 (T-273.15)	J m^{-1} K^{-1} a^{-1}
C_p	Specific heat capacity	$3.1 \times 10^8 \exp(-0.0057T)$	J kg^{-1} K^{-1} a^{-1}
φ	Internal frictional heating		J m^{-3} a^{-1}
G	Geothermal heat flux	55 – 308	mW m^{-2}
D	Flexural rigidity	5.0×10^{20}	N m
δt	Time step	0.03	a
δx_i	Finite difference interval	2×10^3	m
x_{min}	Domain dimensions	-2183000	Gall stereographic
x_{max}		-884000	Gall stereographic
x_{min}		6666000	Gall stereographic
x_{max}		7315000	Gall stereographic

Experiment	**Parameter**	**Area ($x10^5$ km^2)**	**Δ (%)**	**Thick-ness (m)**	**Δ (%)**	**Volume ($x10^5$ km^3)**	**Δ (%)**
Reference		5.615	0	1172	0	6.582	0
Hubbard (2006)		3.290	-41.41	939	-19.88	3.090	-53.06
T -2 °C	Pre-LGM MAAT	5.508	-1.91	1164	-0.72	6.410	-2.61
T +2 °C		5.589	-0.47	1167	-0.48	6.520	-0.95
A_{weert} x 10^{-1}	Sliding	5.537	-1.39	1236	5.45	6.845	3.99
A_{weert} x 10^{1}		5.466	-2.66	909	-22.48	4.967	-24.54
1.5G (136-616 mW m^{-2})	Geothermal heat flux	5.615	0.00	1172	0.00	6.582	0.00
0.5*G* (34-154 mW m^{-2})		5.616	0.02	1173	0.04	6.586	0.06
0.25*G* (17-77 mW m^{-2})		5.667	0.92	1187	1.28	6.728	2.21
0.1*G* (7-31 mW m^{-2})		5.577	-0.68	1229	4.87	6.856	4.16
C – 0.1 (+100%)	Calving	6.595	17.46	1166	-0.50	7.692	16.86
C + 0.1 (-100%)		4.362	-22.31	1072	-8.58	4.675	-28.97
SL_{max} -50 m	Relative sea-level	5.777	2.89	1175	0.21	6.787	3.11
SL_{max} +50 m		4.985	-11.23	1127	-3.86	5.617	-14.66

Period (ka BP)	Total calving losses (Gt)	%	Total surface melt (Gt)	%	Total volume loss (Gt)

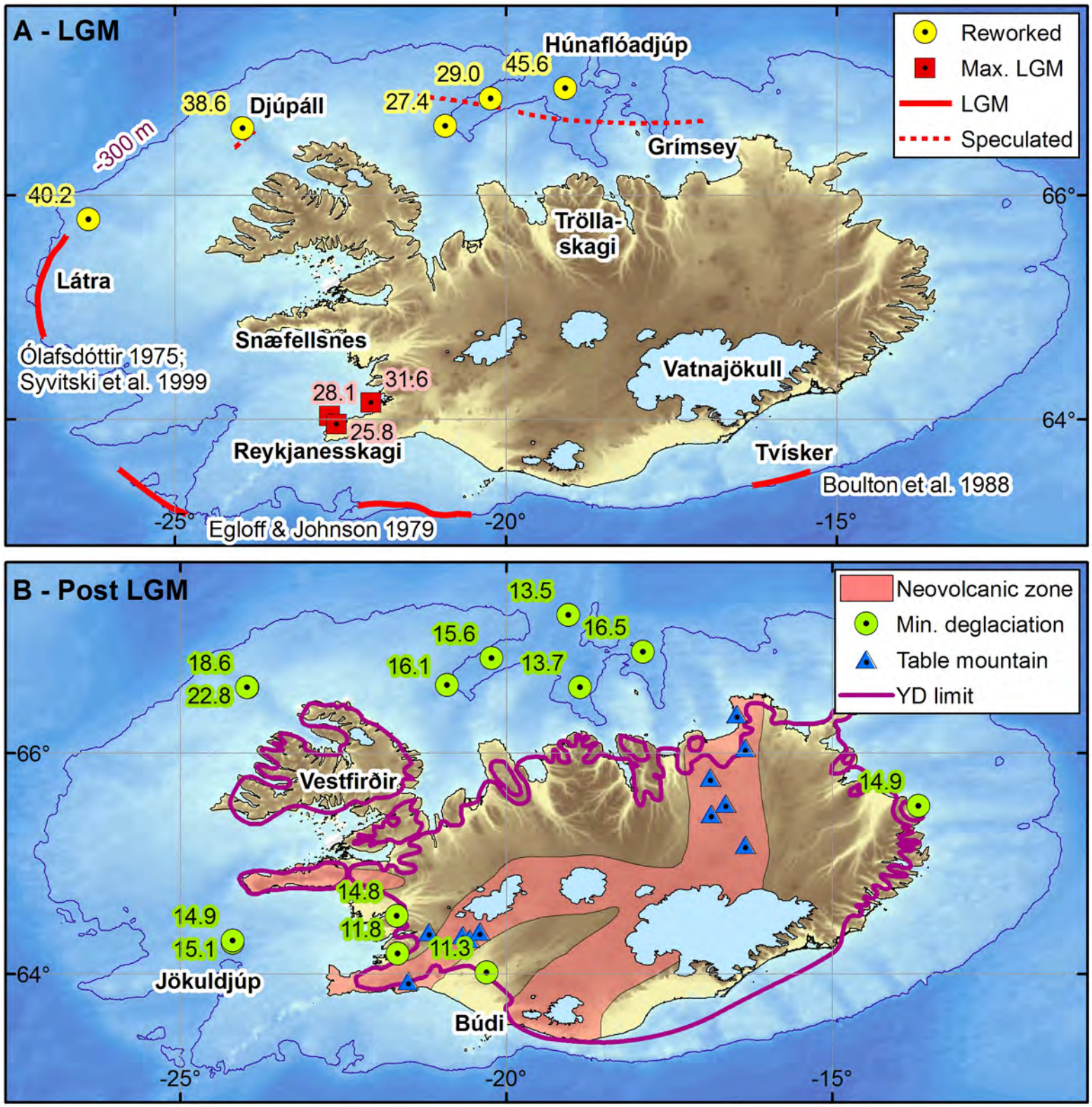
A - LGM
Reworked
Max. LGM
LGM
Speculated
Húnaflóadjúp
45.6
29.0
27.4
38.6
Djúpáll
-300 m
Grímsey
40.2
66°
Trölla-
skagi
Látra
Snæfellsnes
Ólafsdóttir 1975;
Syvitski et al. 1999
Vatnajökull
31.6
28.1
25.8
64°
Reykjanesskagi
Tvísker
Boulton et al. 1988
-25°
Egloff & Johnson 1979
-20°
-15°
B - Post LGM
Neovolcanic zone
Min. deglaciation
Table mountain
YD limit
13.5
16.5
15.6
16.1
13.7
18.6
22.8
66°
Vestfirðir
14.9
14.8
14.9
11.8
15.1
11.3
64°
Jökuldjúp
Búdi
-25°
-20°
-15°

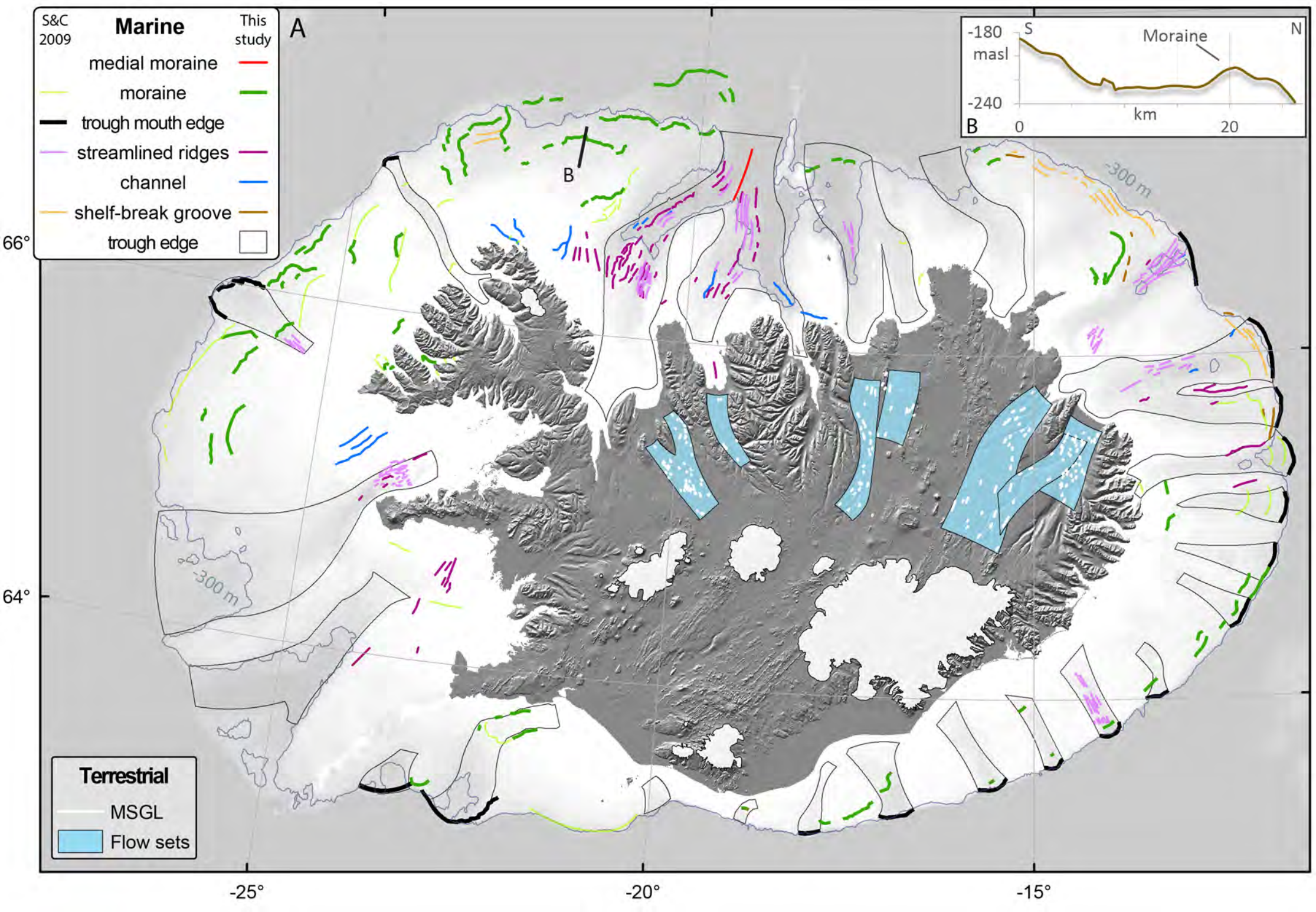
S&C 2009
Marine
This study
medial moraine
moraine
trough mouth edge
streamlined ridges
channel
shelf-break groove
trough edge
A
B
-180
masl
-240
S
N
Moraine
km
0
20
B
-300 m
-300 m
66°
64°
-25°
-20°
-15°
Terrestrial
MSGL
Flow sets

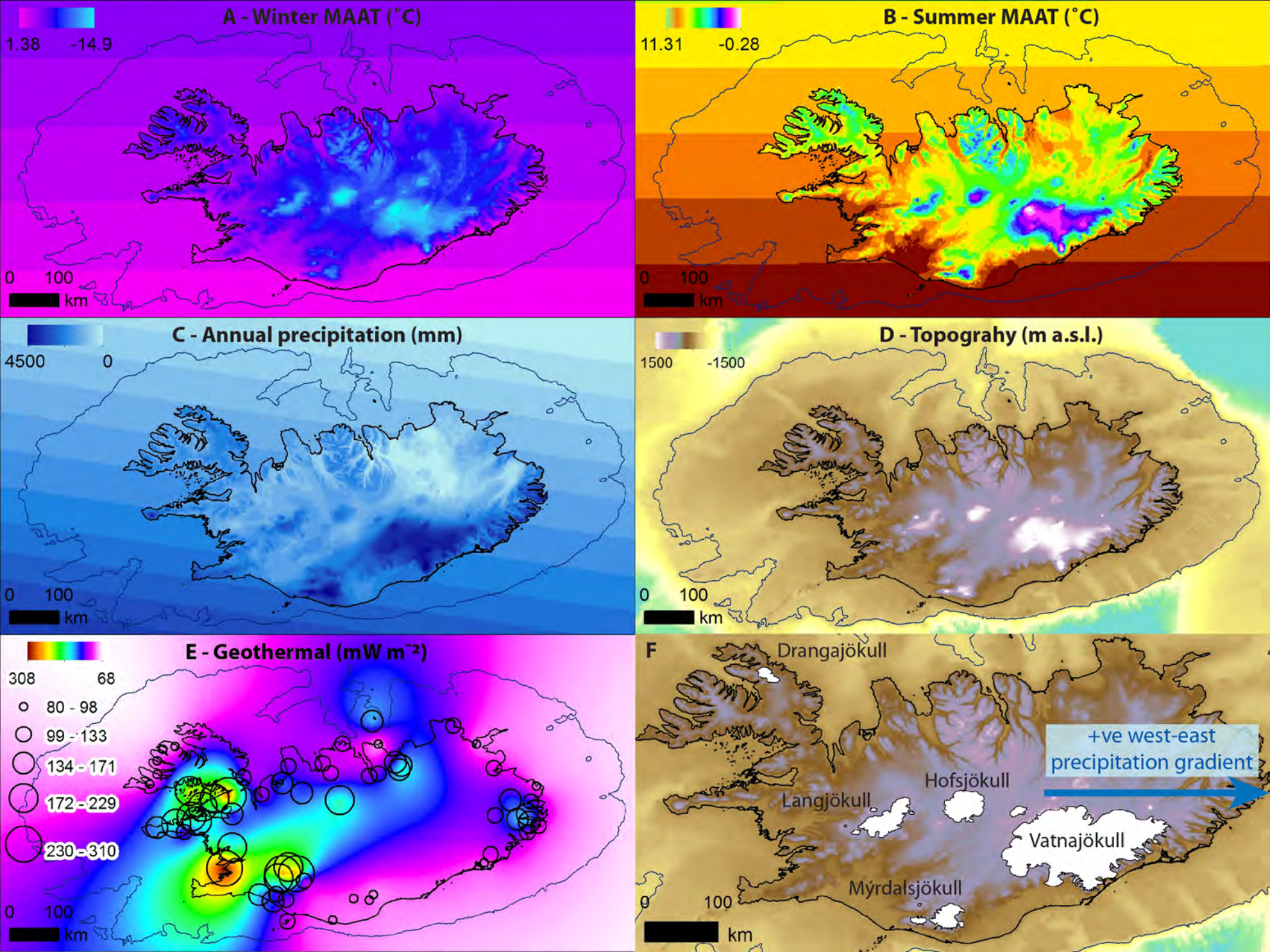
A - Winter MAAT (˚C)
1.38
-14.9
0
100
km
B - Summer MAAT (˚C)
11.31
-0.28
0
100
km
C - Annual precipitation (mm)
4500
0
0
100
km
D - Topograhy (m a.s.l.)
1500
-1500
0
100
km
E - Geothermal (mW m⁻²)
308
68
80 - 98
99 - 133
134 - 171
172 - 229
230 - 310
0
100
km
F
Drangajökull
+ve west-east
precipitation gradient
Hofsjökull
Langjökull
Vatnajökull
Mýrdalsjökull
0
100
km

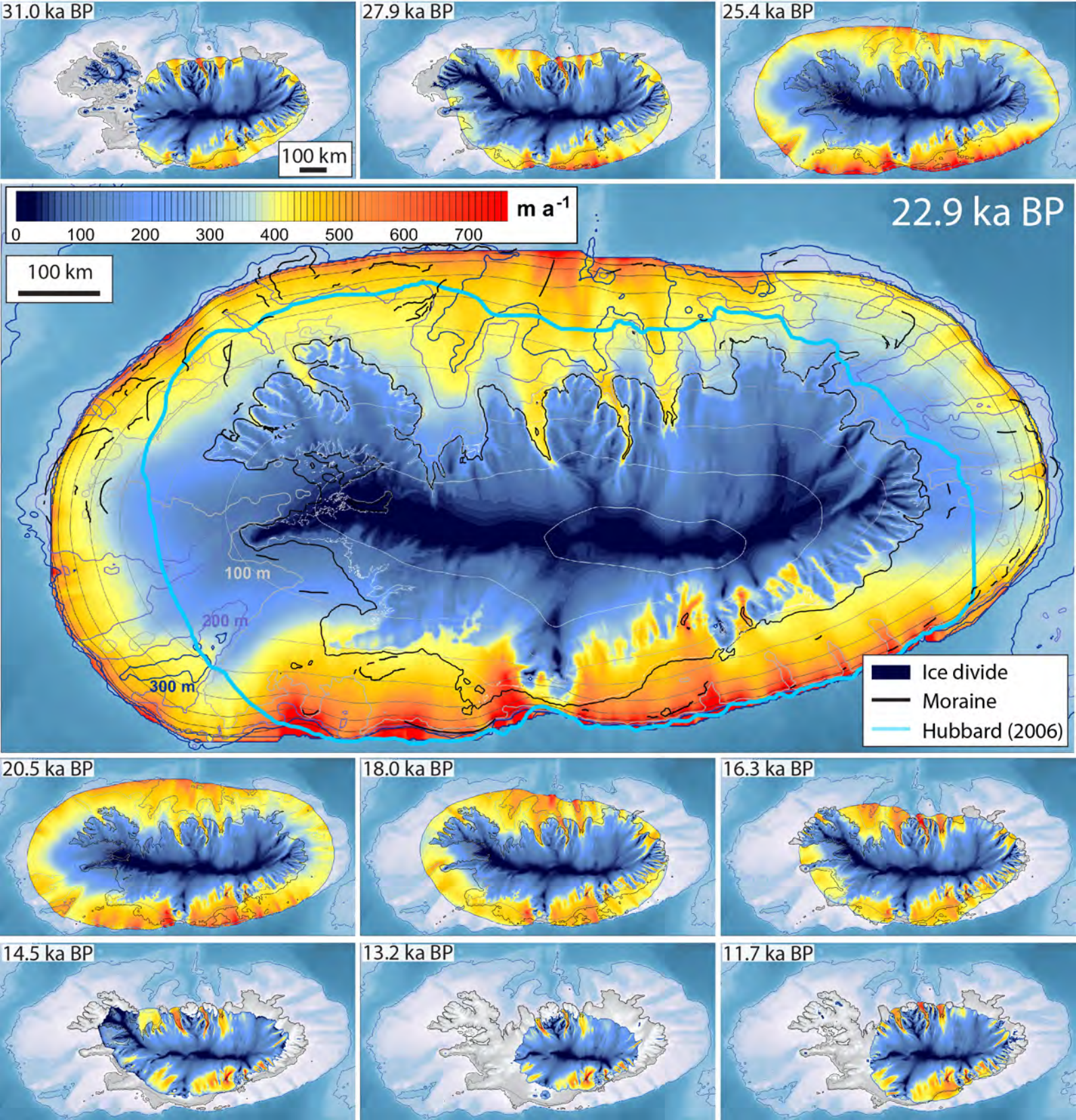
31.0 ka BP
27.9 ka BP
25.4 ka BP
100 km
m a-1
0
100
200
300
400
500
600
700
22.9 ka BP
100 km
100 m
200 m
300 m
Ice divide
Moraine
Hubbard (2006)
20.5 ka BP
18.0 ka BP
16.3 ka BP
14.5 ka BP
13.2 ka BP
11.7 ka BP

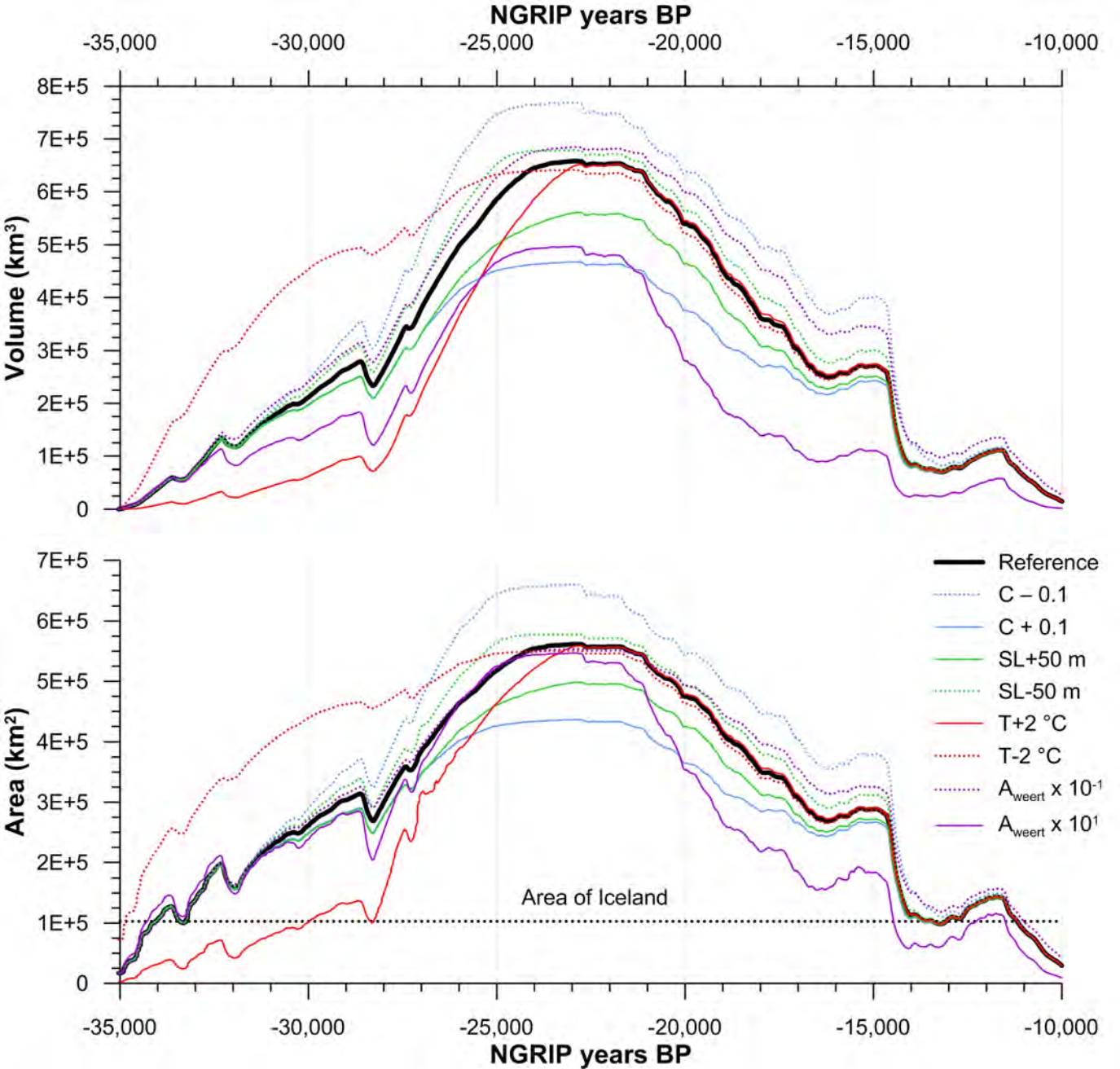
NGRIP years BP
-35,000
-30,000
-25,000
-20,000
-15,000
-10,000
Volume (km³)
8E+5
7E+5
6E+5
5E+5
4E+5
3E+5
2E+5
1E+5
0
Area (km²)
7E+5
6E+5
5E+5
4E+5
3E+5
2E+5
1E+5
0
Area of Iceland
Reference
C – 0.1
C + 0.1
SL+50 m
SL-50 m
T+2 °C
T-2 °C
A_weert x 10⁻¹
A_weert x 10¹
NGRIP years BP

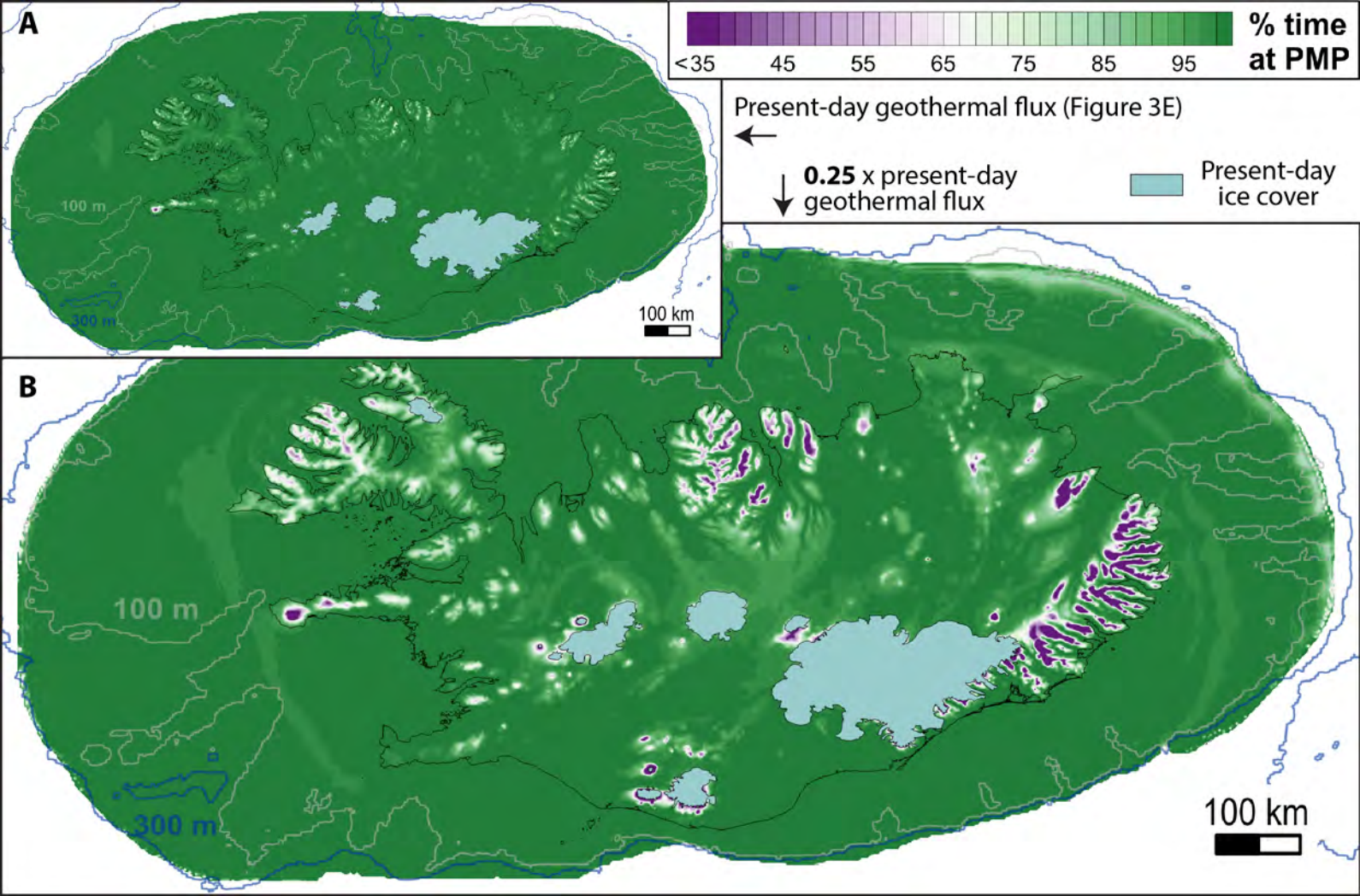
A
<35
45
55
65
75
85
95
% time at PMP
Present-day geothermal flux (Figure 3E)
0.25 x present-day geothermal flux
Present-day ice cover
100 m
300 m
100 km
B
100 m
300 m
100 km

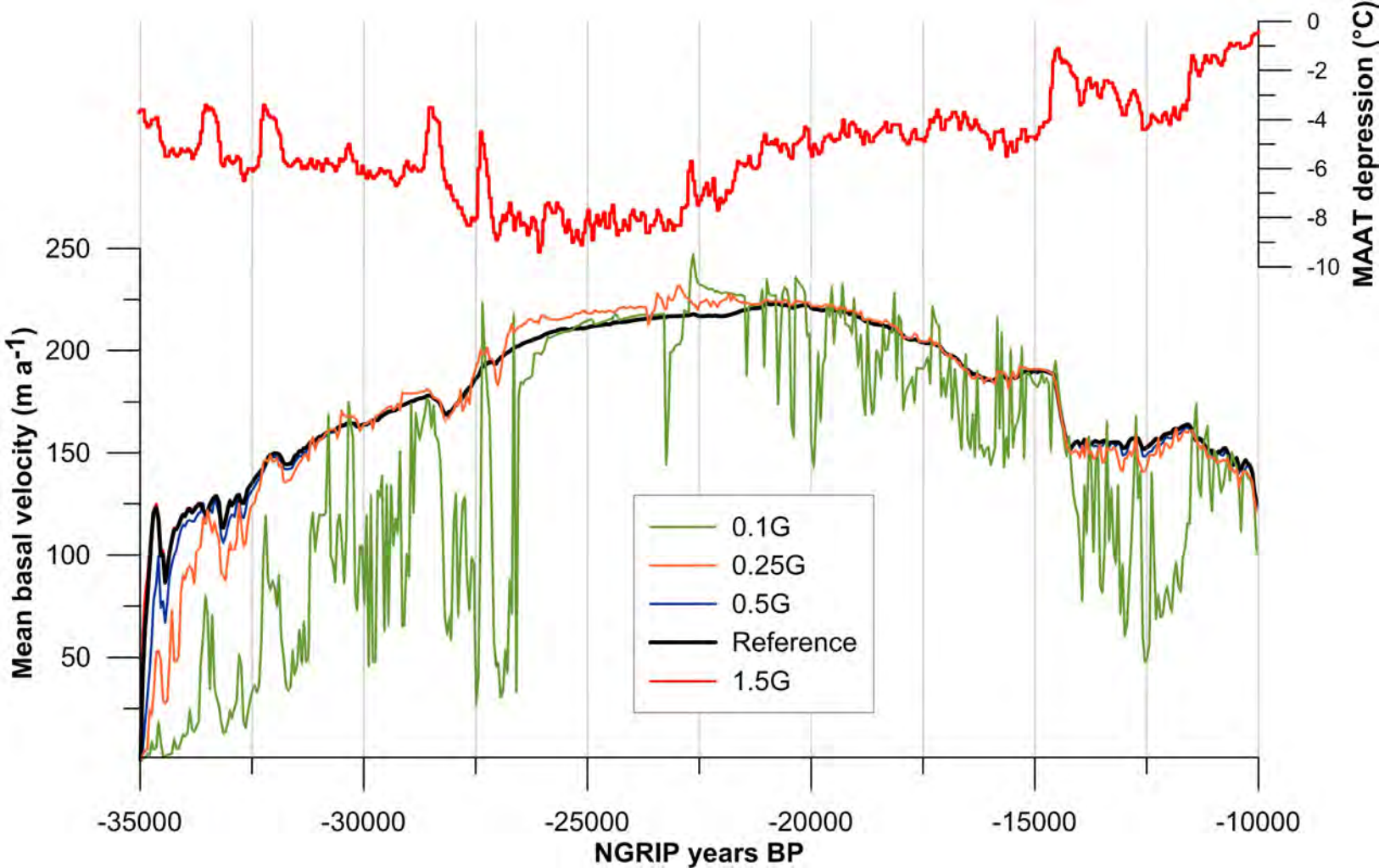
MAAT depression (°C)
0
-2
-4
-6
-8
-10
Mean basal velocity (m a-1)
250
200
150
100
50
0.1G
0.25G
0.5G
Reference
1.5G
-35000
-30000
-25000
-20000
-15000
-10000
NGRIP years BP

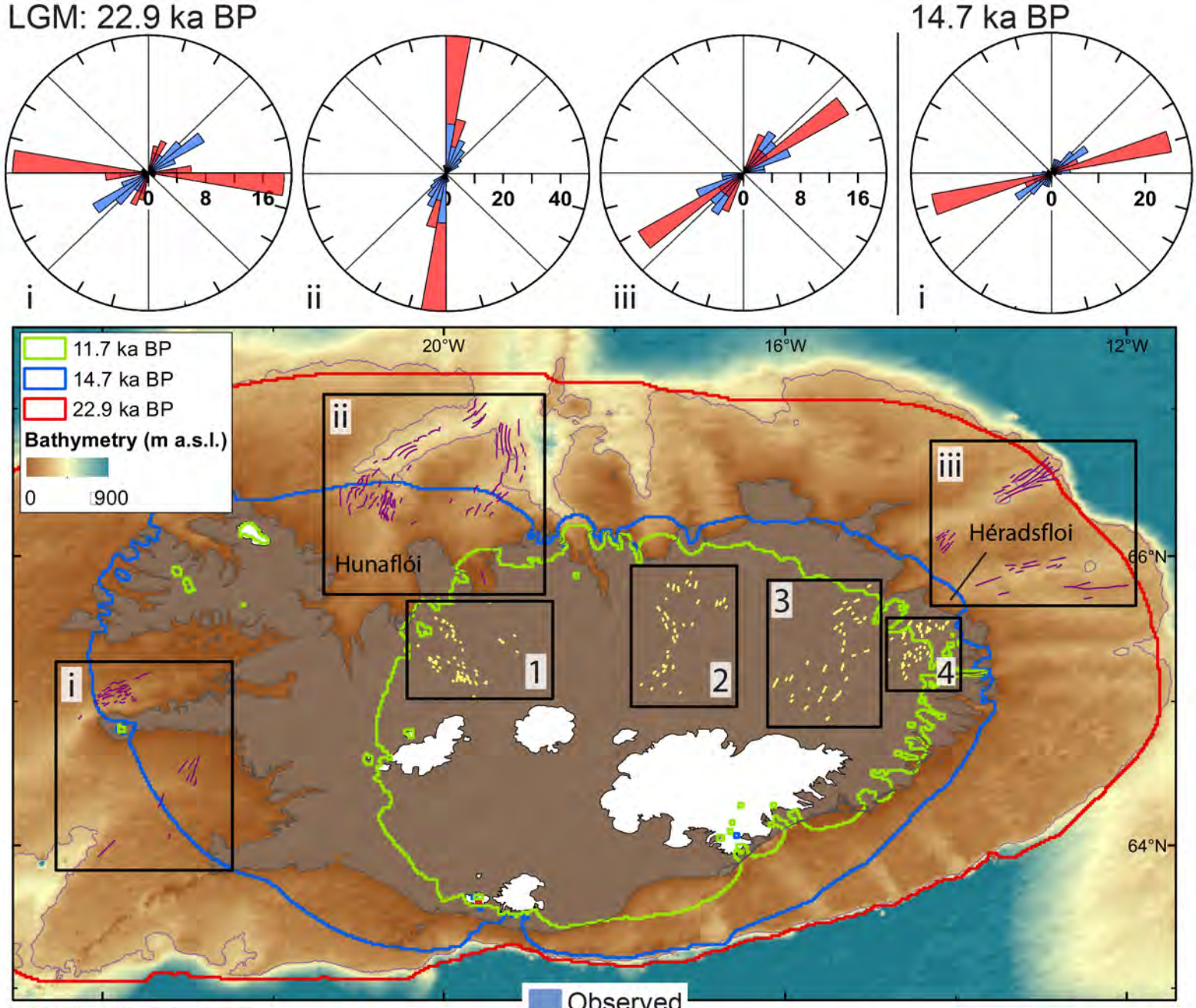
LGM: 22.9 ka BP
14.7 ka BP
i
ii
iii
i
11.7 ka BP
14.7 ka BP
22.9 ka BP
Bathymetry (m a.s.l.)
0
900
20°W
16°W
12°W
66°N
64°N
Hunaflói
Héradsfloi
1
2
3
4
Observed
Modelled
LGM: 22.9 ka BP
1
2
3
4
Younger Dryas: 11.7 ka BP
1
2
3
4

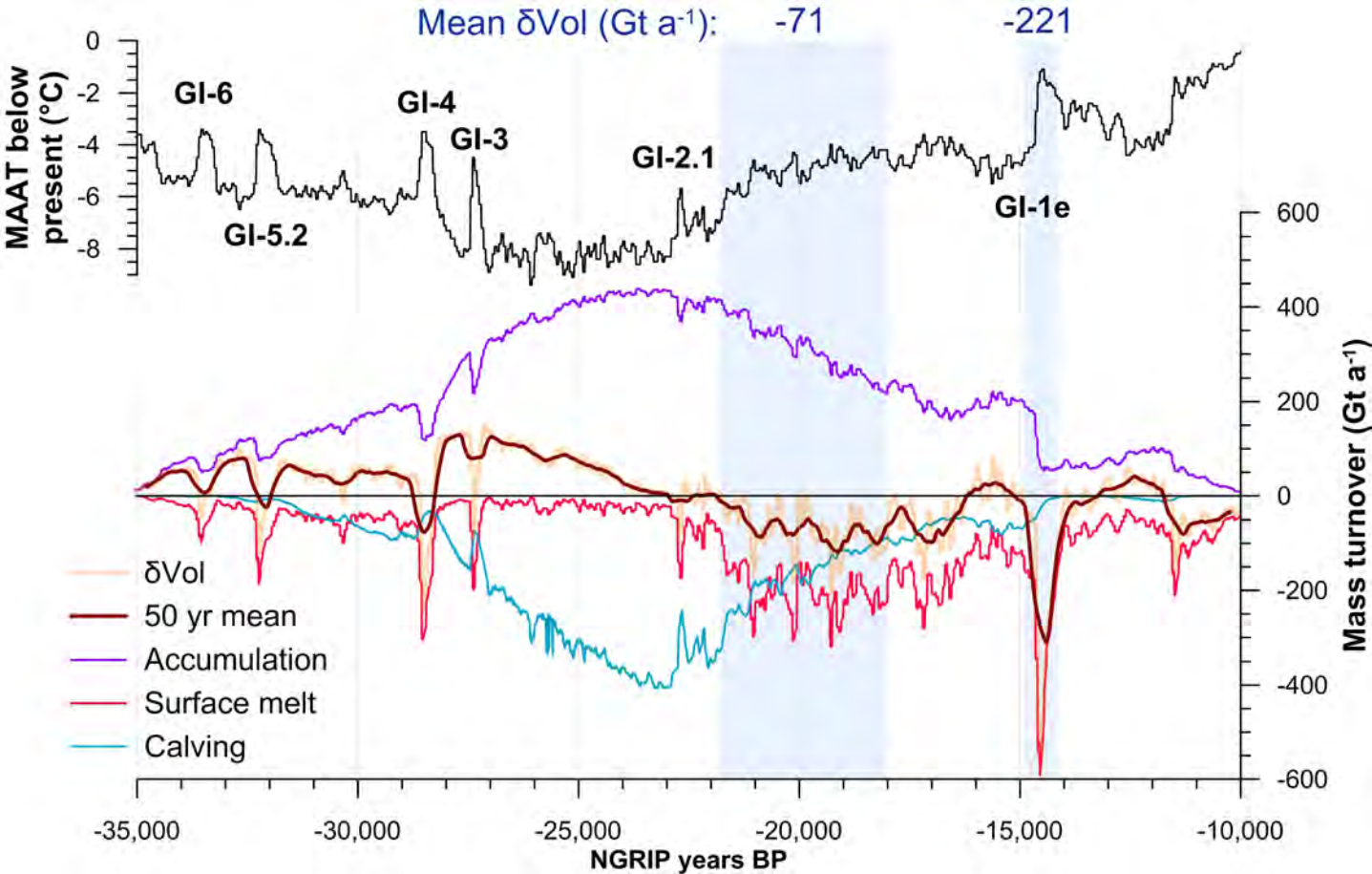
Mean δVol (Gt a-1): -71 -221
MAAT below present (°C)
0
-2
-4
-6
-8
GI-6
GI-5.2
GI-4
GI-3
GI-2.1
GI-1e
600
400
200
0
-200
-400
-600
Mass turnover (Gt a-1)
δVol
50 yr mean
Accumulation
Surface melt
Calving
-35,000
-30,000
-25,000
-20,000
-15,000
-10,000
NGRIP years BP

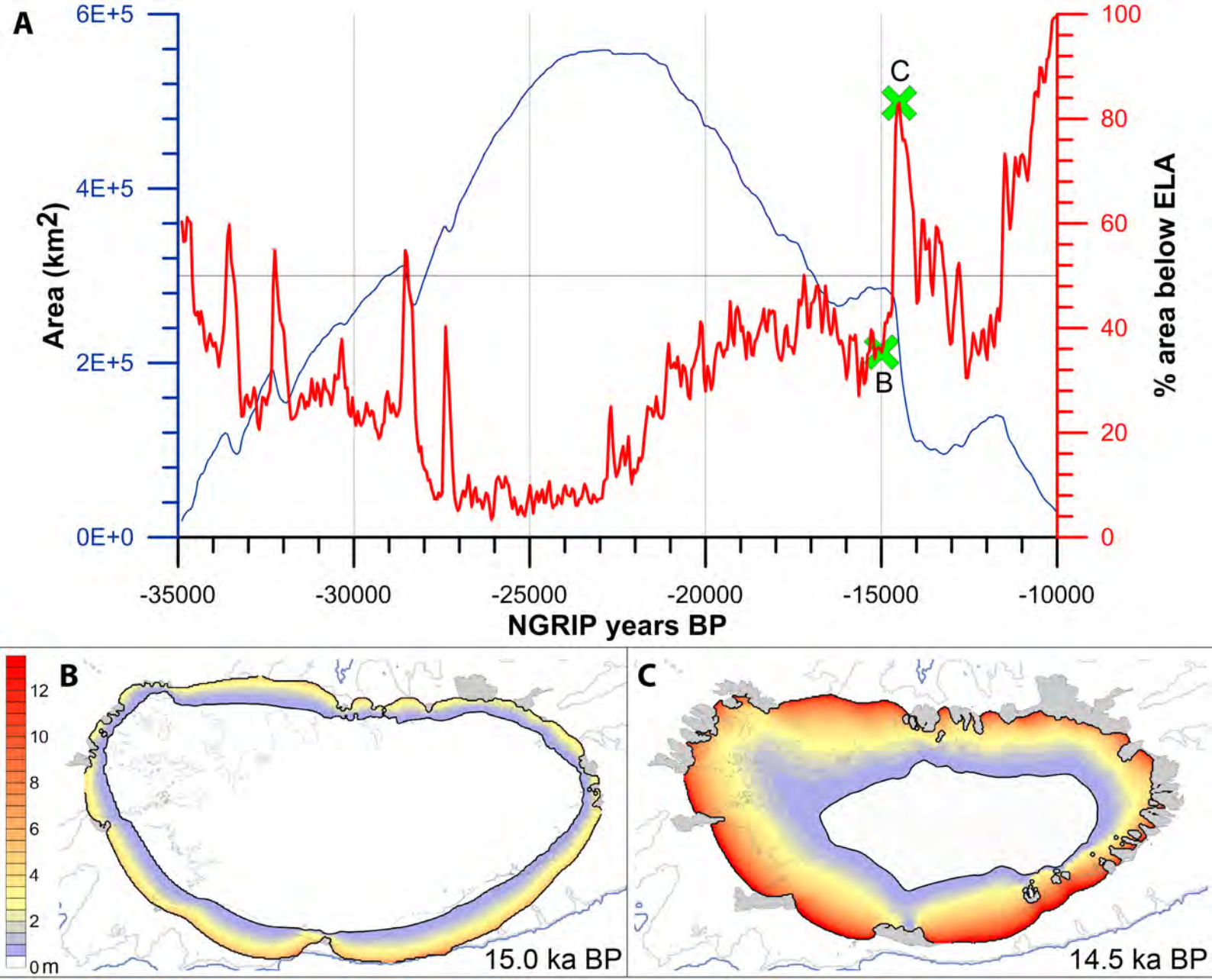
A
6E+5
4E+5
2E+5
0E+0
Area (km2)
100
80
60
40
20
0
% area below ELA
C
B
-35000
-30000
-25000
-20000
-15000
-10000
NGRIP years BP
B
12
10
8
6
4
2
0 m
15.0 ka BP
C
14.5 ka BP

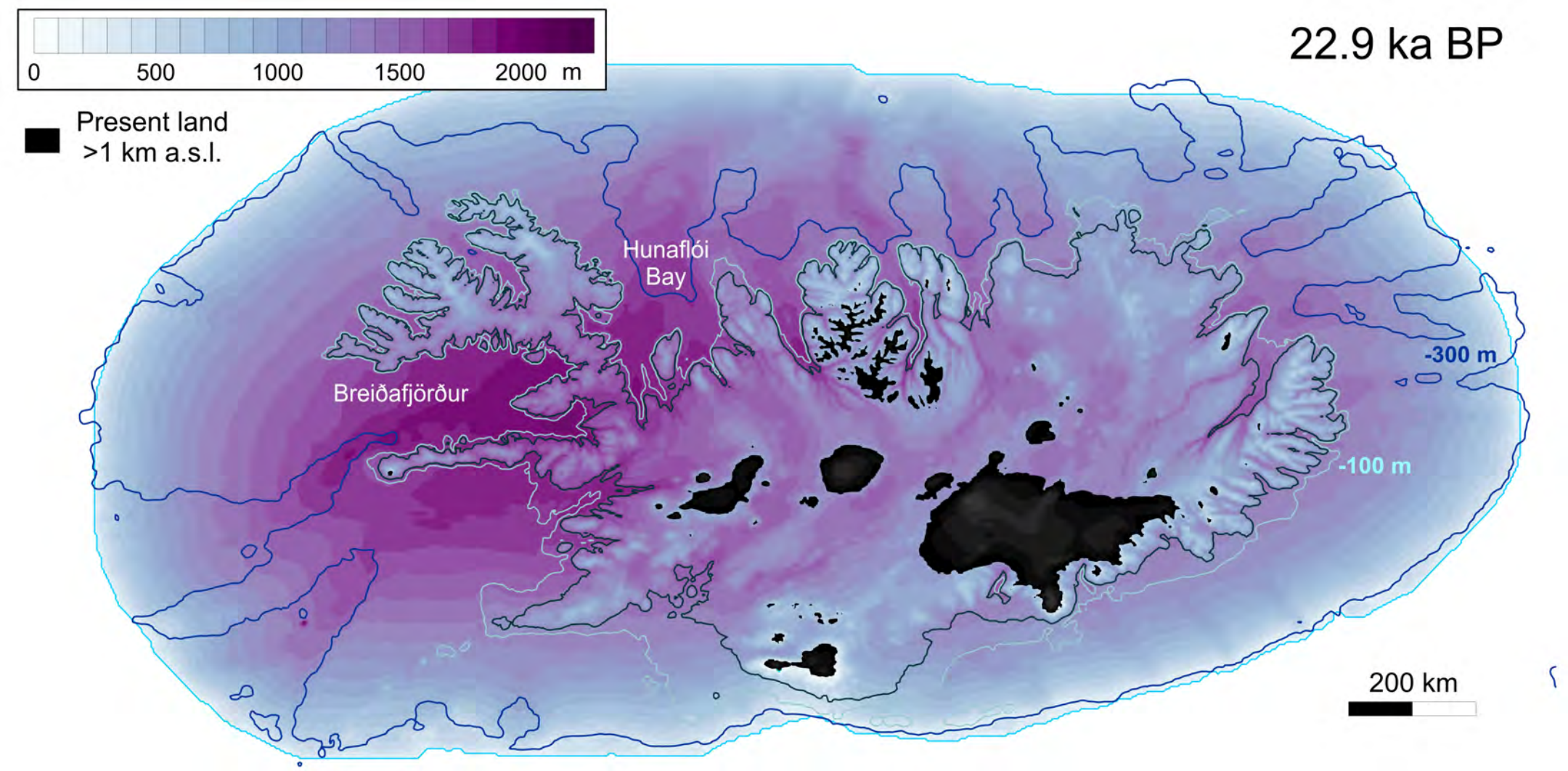
22.9 ka BP
0
500
1000
1500
2000 m
Present land
>1 km a.s.l.
Hunaflói
Bay
Breiðafjörður
-300 m
-100 m
200 km

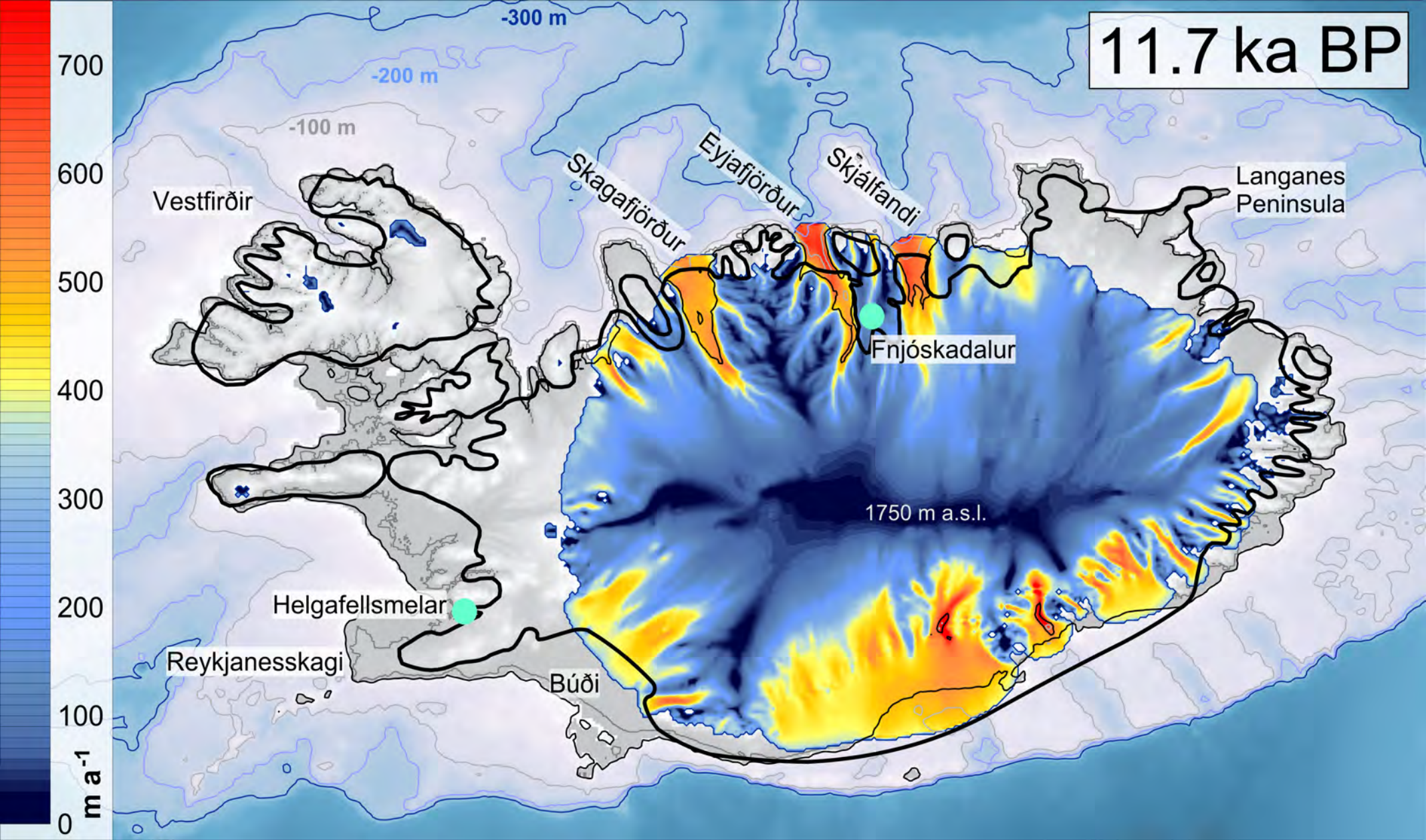
11.7 ka BP
-300 m
-200 m
-100 m
Vestfirðir
Skagafjörður
Eyjafjörður
Skjálfandi
Langanes
Peninsula
Fnjóskadalur
1750 m a.s.l.
Helgafellsmelar
Reykjanesskagi
Búði
700
600
500
400
300
200
100
0
m a-1

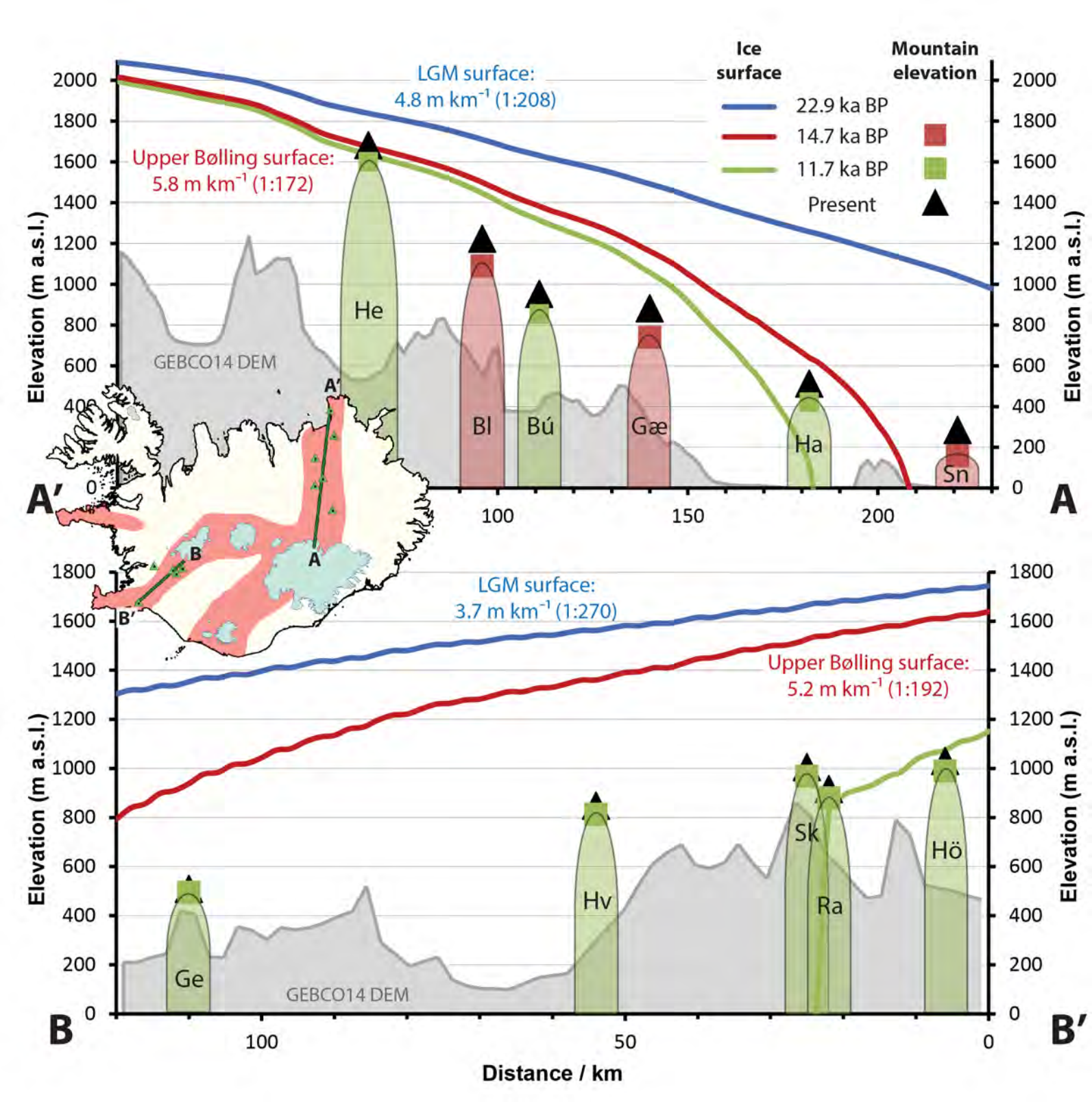
Ice surface
Mountain elevation
22.9 ka BP
14.7 ka BP
11.7 ka BP
Present
LGM surface:
4.8 m km^{-1} (1:208)
Upper Bølling surface:
5.8 m km^{-1} (1:172)
GEBCO14 DEM
He
Bl
Bú
Gæ
Ha
Sn
A′
A
Elevation (m a.s.l.)
LGM surface:
3.7 m km^{-1} (1:270)
Upper Bølling surface:
5.2 m km^{-1} (1:192)
Ge
Hv
Sk
Ra
Hö
B
B′
Distance / km